Elsevier Editorial System(tm) for Applied Clay Science

Manuscript Draft

Manuscript Number: CLAY12322R1

Title: Phosphate capture by ultrathin MgAl layered double hydroxide nanoparticles

Article Type: Research Paper

Keywords: Phosphate removal; Hydrotalcite-like compounds; Nanosheets; Adsorption; Wastewater

Corresponding Author: Professor Gang Pan, PhD

Corresponding Author's Institution: Research Center for Eco-environmental Sciences, Chinese Academy of Sciences

First Author: Chen Liu

Order of Authors: Chen Liu; Meiyi Zhang; Gang Pan, PhD; Laura Lundehøj; Ulla Nielsen; Yi Shi; Hans Hansen

Abstract: Capture of phosphorus from runoff and wastewater is of high priority in order to reclaim phosphorus for food security and to prevent water pollution. Here we report an environmentally friendly method to synthesize ultrathin MgAl layered double hydroxide (LDH) nanoparticles for phosphorus adsorption. Fast co-precipitation of magnesium and aluminum at 25-80 °C in the presence of urea resulted in the desired LDH with variable admixtures of amorphous aluminum hydroxide (16-38%) quantified from solid state 27Al MAS NMR. Freshly synthesized particles appeared as exfoliated single layers that upon drying stacked to form particles with thickness of 3 to 5 nm (four to six LDH layers) and lateral sizes of ~30 nm, as seen by XRD, SEM, TEM, and AFM. Phosphate adsorption on LDH nanoparticles synthesized at room temperature (LDHns-U25) was very fast and reaction reached equilibrium within 15 min at pH 8.5. The freeze-dried LDHns-U25 nanoparticles exhibited phosphate sorption capacity of 98±15 mg P g-1, which is 55% higher than conventional LDH. Phosphate was bound to LDH electrostatically and via inner-sphere surface complexation as evidenced from a combination of 31P MAS NMR spectroscopy, surface potential measurements, IR spectroscopy, and ionic strength effects on phosphate sorption. This study demonstrates that urea-facilitated synthesis of LDH nanoparticles provides fast and high capacity phosphate sorbents with potentials for phosphate recovery from waste waters.

Response to Reviewers: Reviewer(s)' Comments to Author:
Response to comments:
We have carefully revised the paper according to editor’s and the reviewers’ comments. The itemized responses to the comments are listed below.

Reviewer #1:
This manuscript describes phosphate ions capture by LDH powder consisting fine particles. It contains some useful information for readers of Applied Clay Science, but the following items must be considered before

the publication. In addition, this manuscript is rather lengthy. The authors should revise the manuscript more concise.

1. Highlights and Abstract: In the experiment of this manuscript, the authors used LDH powder that is aggregation of fine LDH particles, not colloidal state of fine particle. "LDH nanoparticles exhibit" in Highlights and L26-27 in Abstract, these expressions may mislead readers into believing that colloidal LDHs were used. The authors should correct them.

Response: 'LDH nanoparticles exhibit' has been revised to 'The freeze-dried LDHns-U25 nanoparticles exhibit' in both Highlights and Abstract (Line 31).

2. L36, L311-315: The authors claim LDHns-U25 reached equilibrium rapidly (within 15 min), compared with previous reports in the literature. However, usually ultrasonic treatment is not used before adsorption. The ultrasonic treatment may the cause for quick equilibrium. The authors should give result of kinetics about LDH-Ref, which was LDH prepared by conventional method. By comparison between results of LDHns-U25 and LDH-Ref, the authors can judge what is the cause for quick equilibrium. If the authors do not give the result of LDH-Ref about this, they should not claim quick equilibrium. They can just say that in this condition LDHns-25 reached equilibrium within 15 min in the result section, and cannot claim "fast" reaction in Abstract.

Response: Ultrasonic treatment is usually used to minimize nanoparticle aggregation of LDH suspension (Fang et al. 2015, Zhang et al. 2016). Similar treatment has also been used by magnetic nanoparticles in studies of adsorption of As(V) and As(III) (Cheng et al. 2015). Ultrasonic treatment alone cannot induce the delamination of conventional LDH. Only in the presence of an organic solvent or delaminating agent, for example formamide, can exfoliation take place (Ma et al. 2006, Wei et al. 2014, Wu et al. 2015). The fast adsorption has also been observed by adsortpion of As to ultrathin γ-Fe2O3 nanosheets (Liu et al. 2016), where the capture of As(III) and As(V) increases rapidly in the first 15 min and then plateaus for the next 6 hours. Hence, there is high possibility that the nano-structure and strong surface complexation between the nanoparticles and the phosphate ions are the reasons of fast adsorption (line 278-284).

3. L189-197, 198-200 & 211-213: In the experiment of adsorption, it is difficult to know the concentration of each element. For example, "using 1g L-1" does not mean the concentration of LDH in the finally adjusted solution: readers cannot calculate LDH concentration after the LDH suspension with concentration of 1g L-1 was mixed with unknown volumes of electrolyte and phosphate solution. The authors should clarify the concentration of LDH, phosphate and nitrate in the mixtures after mixing the suspension and solutions.

Response: 30 mL was the total volume of electrolyte and phosphate solution. We added 30 mg LDH powder into the centrifuge tube, thus the LDH concentration in the suspension was 1g L-1. To make this point clearer, we have rewritten the Phosphate adsorption section (section 2.4, line 153-181). Furthermore, to make the passage condense, "Experimental, 2.3 Solid State Characterization" has been shorten in manuscript and details can be found in Supporting Information (line 138-150, Supporting Information line 20-73).

4. L238: Fig 1b and Fig S1 may be the same one. If so, Fig. S1 is not necessary. In addition, "re-stacked" is not appropriate because LDH

sheets were not stacked until dried. Like in the explanation for Fig S1, just "freeze-dried" is more appropriate.
Response: Fig. 1b shows the freeze-dried pristine LDH, while the previous Fig. S1 showed the freeze-dried LDH after phosphorus adsorption. Fig. S1 has been replaced by a combined figure showing XRD patterns of freeze dried MgAl-LDHs before and after phosphate adsorption. The data extracted from XRD characterization is shown in Table S1 (Supporting Information, line 76-80).
"re-stacked" was deleted in the explanation for Fig. 1b (line 207).

5. L256: Mg/Al ratios of 1.97, 1.90 and 2.10 may be calculated from the result of ICP-OES, but it is not clear. Clarify this.
Response: Yes, and the text has been clarified (Line 223-225).

6. L276: SEM images of LDH-Ref should be shown. In addition, Fig. S3 was not used in the text. Is Fig. S3 really necessary?
Response: To make the manuscript more concise, we have moved the previous three SEM images to the Supporting Information and combined with the SEM images of LDH-Ref to produce a new Fig. S3 (Supporting Information, line 95-97).

7. L302-304: AFM images were provided only for LDHns-25. For comparison, at least AFM images of LDH-Ref should be provided. Crystallite size in the direction of 00l can be calculated from the result of Fig. 1b. The authors should compare the thickness values obtained from AFM with the above-mentioned crystallite sizes. In addition, what is "ScanAsyst mode"? It is not common word. Moreover, what is the difference between (a) and (b)?
Response: AFM images of LDH-Ref has been shown in Fig. S4 (Supporting Information, line 98-102). For comparison, the AFM image of LDH-Ref along with the corresponding height profile is shown in Fig. S4. The size of LDH-Ref is larger compared to LDH nanoparticles, with diameter of 100-150 nm and thickness of higher than 14 nm (line 268-271).
The thickness values obtained from AFM were compared with d003 in manuscript (Line 260-264). The d003 of LDHns-U25 is 0.817 nm (Table S1), which is close to the thickness of single metal hydroxide layer with interlayer (0.8 nm) (Yu et al., 2015). The AFM images reveals a particle thickness of 3 to 5 nm, containing four to six layers.
ScanAsyst mode is an image mode of AFM (Bruker). It is a PeakForce Tapping® based image optimization technique that enables every user to create the highest resolution AFM images using single-touch scanning (Supporting Information 55-57). One can visit the website 'https://www.bruker.com/products/surface-and-dimensional-analysis/atomic-force-microscopes/modes/modes/imaging-modes/scanasyst.html".
Fig.4 (a) and (b) are two views of LDHns-25, but with no big differences between them. Thus, we delete the previous Fig. 4(a) and combine the previous Fig.4(b) with Fig. 3 to produce Fig. 3(d) (line 254-258).

8. L330-331: In this part, do the authors mention contribution of adsorption on external surface of LDH particles? Do the authors also imply extra adsorption that does not come from exchange for interlayer anions? The sentence should be revised clearly.
Response: we delete the puzzling sentence and discuss the adsorption mechanism in detail in the following sections.

9. L338-339: This sentence is puzzling.

Response: The sentence has been revised to “Thus, desorption from LDH nanoparticles is low, hence increasing the potential of the LDH materials for water cleaning.” (Line 306-308).

10. L 342: What does 73 to 42 mg g-1 refer to? In Fig 6b, data is expressed by %.
Response: We are sorry for the mistake in Fig. 6b, the unit should be mg g-1. This has been revised in the manuscript (line 327).

11. L345-347: In this part, do the authors mention contribution of adsorption on external surface of LDH particles? The sentence should be revised clearly.
Response: This refers to the adsorption on both external and internal surface of LDH particles.

12. L348-349: When pH increase, amount of OH- ions increase. Therefore, competition with OH- can be a cause for drop of phosphate adsorption too. The authors should consider this possibility.
Response: The sentence has been revised to “Thus, the change in charge of phosphate ion, the LDH metal hydroxide layers and competition with OH- jointly cause adsorption to decrease with increasing pH. Furthermore, competition with carbonate is also more prevalent at high pH due to the unfavorable shift in the CO2-equilibrium (Lundehøj et al, 2019)” (Line 317-320).

13. L377: It should be explained how to calculate contribution of AlOH.
Response: We assign the broad resonance at □iso(31P) □ -9 ppm to phosphate adsorbed to AOH and this P-AOH resonance constitute 6(4) to 12(6) % of the total P adsorbed, cf. Fig. 6. Thus, phosphate sorbed to the AOH component amounts to less than 15% of the sorption maximum (Line 344-353). The previous estimated calculation has been deleted.

14. L382: Why are not these resonances seen for the samples of this article?
Response: We assign the broad resonance at □iso(31P) □ -9 ppm to phosphate adsorbed to AOH and possibly a small amount of an amorphous aluminum phosphate (AlPO4) phase based on our recent study of phosphate adsorption on ZnAl-LDH in acidified waste water sludge. We have revised the text and added an assignment based on our recent study of phosphate adsorption by ZnAl-LDH in waste water (Lundehøj et al 2019)(Line 344-353). The text has been modified and our previous assignment based on earlier literature studies deleted.

15. L431: This sentence is puzzling. On L430-431, the authors seem to use the data of maximum adsorption amounts calculated from Langmuir equation. These maximum amounts includes adsorption on external surfaces, exchange for interlayer anions and adsorption to AlOH. Does "other mode" on L431 refer to anything other than these?
Response: “other mode” refers to the mode that is different from electrostatic bonding. It could be exchange for interlayer anions, surface complexation, or adsorption on AOH. There was a mistake in line 402 and the sentence was revised to “A simple calculation accounting for the charge of the LDH interlayer and the charge of the phosphate anion provides an estimate of the maximum amount of phosphate (HPO42-) that can be adsorbed due to electrostatic bonding (Supporting Information).” (Line 400-403).

16. L435-439: Discussion is not enough. The authors discuss contributions from each element: adsorption sites on external surface, exchange for interlayer anions and adsorption on AlOH. The authors should discuss the relationship among them. Especially, relationship between actual adsorption amounts and theoretical anion exchange capacities (AEC), which are proportional to Al amount (not maximum adsorption amounts calculated from Langmuir plot) should be discussed. When data in Tables 2 and 3 are compared, on the condition that phosphate ions are divalent, phosphate adsorption amounts are beyond AEC in the case of LDHns-F and LDHns-25. As for LDH-Res, the phosphate adsorption amounts was close to AEC. (Practical AEC will be equivalent to amount of nitrate ions in the interlayer space. Therefore, it is strongly recommended that the authors should provide data of nitrate contents in samples.) The authors should discuss relationship of the above-mentioned adsorption sites quantitively.
Response: We have measured nitrate content in the samples, but the values are not trustworthy due to long storage problem. We have estimate calculated the nitrate content based on the actual Mg and Al content in LDH samples. For LDHns-F and LDHns-U80, the theoretical AEC of LDH nanoparticles are close to adsorption capacities. For LDHns-U25, adsorption capacity from Langmuir fitting is 12% higher than calculated adsorption capacity. Since we do not have the AOH value for LDH-Ref, we use Mg and Al content from ICP-OES to calculate theoretical AEC, which is 40% higher than adsorption capacity. Wang et al. (2009) showed that Mg:Al ratio of 2:1 and 3:1 LDH have both vertical and horizontal orientations of interlayer nitrate ions. The interlayer nitrate with an orientation perpendicular to the hydroxide sheets can exchange with phosphate more readily while an orientation parallel to the sheets cannot. Hence only part of nitrate ions can be exchanged with phosphate.

Samples	Mg/Al in LDH	calculated AEC (mmol/g)	calculated adsorption capacity (mg P/g)	Langmuir fitting adsorption capacity (mg P/g)	Molecular formula
LDHns-F	2.63	3.05	94.7	89.6	Mg2.63Al(OH)7.25NO3.2H2O
LDHns-U25	3.06	2.83	87.9	98.3	Mg3.06Al(OH)8.13NO3.2H2O
LDHns-U80	2.50	3.13	96.9	97.6	Mg3.06Al(OH)7NO3.2H2O
LDH-Ref	1.90	3.44	106.5	63.5	Mg1.90Al(OH)6NO3.2H2O

17. L433 & 438: Does "surface" refer to external surface of LDH particles?
Response: 'L433': We cannot tell if the adsorption takes place on the external surface or internal surface based on 31P MAS or both. There are few weak spinning side bands (Fig.6, line 355) but we cannot specify them (line 342-344).
'L438': Surface complexation refers to both internal and external surfaces of LDH nanoparticles.

18. L447: Data of Kuzawa et al. is missing in Table S4.
Response: Added (Supporting Information, Table S4).

19. L451-452: In Table S4, data of Mg-Al LDHs other than those of this manuscript are not shown. Zn-LDH and Mg-Mn LDH are shown in Table S4, but Zn and Mn are heavy element. Therefore, adsorption amount per unit weight is unfair. The authors should compare the data of Mg-Al LDHs (e.g. 47.3 mg/g for granular HTAL (LDH content was ca. 90%) in Kuzawa, K. et al. (2006) Chemosphere 62, 45; 2.37mmol/g (73.4 mg/g) in Ookubo, A. at al. (1993) Langmuir 9, 1418) , and then claim whether the authors' sample

show high adsorption ability or not. In addition, what does "high site density" exactly mean? Where are these sites? Explain clearly.
Response: Zn-LDH and Mg-Mn LDH were deleted and Kuzawa et al. (2006), (Ookubo et al. 1993) were added in Table S4. The LDHns-U25 show higher adsorption capacities compared to granular HTAL, HTAL, Mg-Al LDH and MgAl-NO3 LDH in the literature (Kuzawa et al. 2006, Ookubo et al. 1993, Yang et al. 2014, Khitous et al 2015) (Table S4, Supporting Information, line 111-114). "High site density" refers to a high density of adsorption sites that are not accessible in thicker LDH particles (line 428-429) (Fang et al, 2015).

20. L477: What is "coatings on porous host particles"? This is not explained in Results and Discussion section. In Conclusions section, the authors should not mention things that are not explained in the earlier sections.
Response: This part has been deleted.

Reviewer #2:
Chen Liu et al present an interesting paper about the reactivity of ultrathin hydrotalcite LDH with phosphate. In fact, the initial product is a mixture of LDH and a significant amount of aluminum hydroxide gel that was detected with RMN. The authors provide an impressive amount of experimental data including XRD, TEM, SEM, AFM, FTIR, surface potential measurements. The data are analyzed cautiously and the originality of the work is related to a relative increase of phosphate adsorption due to the special nature of the initial product. Due to the high quality of the data, the paper is suitable for publication in Applied Clay Science. However, some points are not completely clear and the paper could be improved by giving answers to the following questions:
> Main remarks:

1) Are you sure that the phosphate removal capacity are given in mg P-PO4 g-1 unit and not in mg7 PO4 g-1? I ask you this question because I am a bit surprised by some of the values provided for the "classical" hydrotalcite reference sample (synthesised by coprecipitation) and for ferrihydrite in Table S4.
A P-PO4 removal capacity of 63,5 mg P-P04 g_1(classical hydrotalcite) would correspond to a PO4 removal capacity of about 190 mg PO4 g-1. This value is relatively high and I saw much lower values in literature data. Please provide also other values for classical hydrotalcite in Table S4. Same remarks for ferrihydrite, I am very surprised by the value of 77,2 mg P-PO4 that would correspond to a PO4 removal capacity of about 235 mg PO4 g-1. More recent references concerning ferrihydrite maximal values for ferrihydrite of about 80 mg P04 g-1 at pH of 7. Please check this important point in all the data given in the paper, e.g. page 4 the value of 45,9 mg g-1, is it P-PO4 or PO4?
Response: Yes, the phosphate removal capacities are given in mg P g-1, not mg PO4 g-1 in this study. Same measures have been used for ferrihydrite and nano-Mg(OH)2 in page 4. In Table S4, the values for granular HTAL, HTAL, MgAl-NO3 LDH, CaAl-LDH, Phoslock, gibbsite, AOH, goethite, ferrihydrite, Fe-Al-Mn oxide are all given in mg P g-1. The values for classical hydrotalcite are provided in Table S4 (Supporting Information, line 111-114).

2) The XRD data (modification of the c spacing or d003) should be more cautiously compared to literature data concerning the interaction of hydrotalcite with PO4. I saw controversial data concerning the intercalation of PO4 into MgAl LDL. Some papers report some variation of

the c spacing and other data do not. The variation of the d003 spacing should be discussed with more details in the paper. It seems that the ultrathin LDH present a initial c spacing different from the classical LDH. This may be discussed, is it due to the synthesis or is it due to a variation of the Mg-Al ratio. Ultrathin LDH seems to present a more opened initial structure that may incorporate more easily PO4.
Response: There is controversial data showing that d spacing decreased (from 8.37 Å to 7.61 Å) after phosphate adsorption on MgAl-NO3 LDH and the paper claimed that this is because phosphate ion is smaller than nitrate (Khitous et al, 2015). However, more evidence in literature show intercalation of phosphate on colloidal MgAl-NO3 LDH nanosheets (d003=8.4 to 10.1 Å) (Koilraj et al. 2013), MgAl-CO3 LDH (d003=7.6 to 12.1 Å) (Wang et al. 2010), ZnAl-NO3 LDH (d003=8.8 to 11.1 Å) (He et al. 2010). Our data show a slight increase of d003 (LDH-Ref: d003=7.77 to 8.11 Å; LDHns-U25: d003=8.17 to 8.56 Å) after phosphate adsorption (see Figure below and Table S1). The little change in interlayer spacing after intercalation is in agreement with the findings in Gillman et al. (2008). This could be attributed to non-uniform distribution of phosphate/water in the interlayers (Gillman et al. 2008) (line 408-410). Wu et al. (2005) present a d003 value of 8.27 Å for classical MgAl-NO3 LDH, which is higher than that of LDH-Ref but close to the d-spacing of LDH nanoparticles in our study.

3) Do you believe to the co-intecalation of PO4 and NO3 presented in the last figure of the paper or is it a simplified view. FTIR seems to indicate that NO3- is not fully replaced by PO4. A quantification of the quantity of NO3- species released in solution would give a more accurate answer to this question.
Response: In our study, NaNO3 was added as electrolyte solution. The concentration of nitrate in the solution reduced from 10 to 3.4 mmol/l after phosphate adsorption. The concentration of nitrate added in the solution is much higher than that of phosphate, thus competitive adsorption exists between nitrate and phosphates anions (line 395-399).

4) Page 13, a better explanation between the MgAl ratio "expected" and measured (Table 2) is missing. Is it the difference between the quantity introduced in the initial solution and the real value taking into account the presence of the Al hydroxide. I am not a specialist of NMR but how accurate are the quantitative estimation of Al hydroxide? The Al(OH)3 phase was not detected with other techniques, even with TEM, this is a bit surprising for a compound representing more than 10 % of the mixture.
Response: The relation between expected and measured Mg:Al ratios has been clarified (line 223-228). The initial Mg:Al ratios measured by ICP-OES are very close to the synthesis mixture (2:1). The real ratios take into account the presence of Al in AOH from 27Al SSNMR (Table 2). The difference between the measured value and real value is because of the presence of AOH.
The Al(OH)3/AOH (Amorphous aluminum hydroxide) phase is amorphous or poorly crystalline, hence it will not be detected by PXRD. Furthermore, the particle size is small so they are difficult to observe in TEM. 27Al SSNMR is one of the most reliable methods for identification of AOH. The AOH concentrations above 3-5 % Al can be quantified by 27Al SSNMR, as reported and discussed earlier by Nielsen and co-worked (Pushparaj et al. 2015, Staal et al. 2017).

5) You did not compare the kinetics data of ultrathin LDH with the reference classical LDH. Does the classical LDH adsorb PO4 also so quickly (15 min?). If not it should be mentioned.

Response: The phosphate adsorption on ultrathin LDHns-U25 is fast, compared to classical MgAl-LDH as reported in the literature, the equilibrium time will take from 40 min to a few hours(Das et al. 2006, Yang et al. 2014, Khitous et al. 2015) (Line 280-283).

> Minor remarks
> 1)line 48 "us" is "as"
> 2)space are missing lines 123, 133 and other problems with brakets
> 3) line 226 (001) is (003) ?
> 4) lines 230-231 sentence is unclear, please modify it. "ration" is "ratio".
Response: Revised (line 48, 123,132, 193, 197-200)

Reviewer #3:
1. I doubt the stability of LDH at pH 3.
Response: The LDH is not stable at pH 3. In the pH effects experiment, we started at pH 7 to avoid the dissolution of LDH under 5 (Ookubo et al. 1993).

2. The PO4 loaded LDH may be characterized.
Response: The phosphate loaded LDH was characterized by XRD (Supporting Information, Fig. S1, Table S1, line 76-80). Our data show a slight increase of d003 (LDH-Ref: d003=7.77 to 8.11 Å; LDHns-U25: d003=8.17 to 8.56 Å) after phosphate adsorption. The little change in interlayer spacing after intercalation is in agreement with the findings in Gillman et al. (2008). This could be attributed to non-uniform distribution of phosphate/water in the interlayers (Gillman et al. 2008) (line 408-410).

3. The following references may be referred in the introduction part of the manuscript.

> 1. Physico-Chemical Characterization and Adsorption Behaviour of Calcined Zn/Al Hydrotalcite- Like-Compound (HTlc) Towards Removal of Fluoride from Aqueous Solution. J. Coll. Interf. Sci. 261 (2003) 213-220.
> 2. Calcined Mg-Fe-CO3 layer double hydroxide as an adsorbent for the removal of selenite. J. Coll. Interf. Sci. 316 (2007) 216-223.
> 3. A Review on Recent Progress, Challenges and Perspective of Layered Double Hydroxides as Promising Photocatalysts, J. Mater. Chem. A,4 (2016), 10744-10766.
Response: Thank you for your recommendations. These references have been referred in the introduction part of the manuscript (line 57-58).

> Minor comments from the associate editor:
> - Correct terminology should be in agreement with the guide for authors, for instance abbreviations should not contain final 's' even in for plural in agreement with the guide for authors, please replace LDHs by LDH
Response: Checked

Reference
Cheng-Hua, L., Ya-Hui, C., Tsan-Yao, C., Yuan, T., Hui, L., Ming-Kuang, W. and Wei, Z.,2015. Mechanism of Arsenic Adsorption on Magnetite Nanoparticles from Water: Thermodynamic and Spectroscopic Studies. Environmental Science & Technology 49(13), 7726-7734.
Das, J., Patra, B.S., Baliarsingh, N., Parida, K.M., 2006. Adsorption of phosphate by layered double hydroxides in aqueous solutions. Appl. Clay Sci. 32, 252-260.

Fang, L., Huang, L., Holm, P.E., Yang, X., Hansen, H.C.B., Wang, D., 2015. Facile upscaled synthesis of layered iron oxide nanosheets and their application in phosphate removal. J. Mater. Chem. A 3, 7505-7512.
Gillman, G., Noble, M. and Raven, M.D.,2008. Anion substitution of nitrate-saturated layered double hydroxide of Mg and Al. Applied Clay Science 38(3-4), 179-186.
He, H., Kang, H., Ma, S., Bai, Y., Yang, X., 2010. High adsorption selectivity of ZnAl layered double hydroxides and the calcined materials toward phosphate. J. Colloid Interface Sci. 343, 225-231.
L. Lundehøj H.C. Jensen, L. Wybrandt, U. G. Nielsen, M.L. Christensen, C. A. Quist-Jensen., 2019. Layered Double Hydroxides for phosphorus recovery from acidified and non-acidified dewatered sludge. Water Res. https://doi.org/10.1016/j.watres.2019.01.004
Khitous, M., Salem, Z. and Halliche, D.,2015. Removal of phosphate from industrial wastewater using uncalcined MgAl-NO3 layered double hydroxide: batch study and modeling. Desalination & Water Treatment 57(34), 1-12.
Koilraj, P., Antonyraj, C.A., Gupta, V., Reddy, C.R.K. and Kannan, S.,2013. Novel approach for selective phosphate removal using colloidal layered double hydroxide nanosheets and use of residue as fertilizer. Applied Clay Science 86(8), 111-118.
Liu, R., Liu, J.F., Zhang, L., Sun, J. and Jiang, G.,2016. Low Temperature Synthesized Ultrathin γ-Fe2O3 Nanosheets Show Similar Adsorption Behaviour for As(III) and As(V). Journal of Materials Chemistry A 4(20), 7606-7614.
Ma, R.Z., Liu, Z.P., Li, L., Iyi, N., Sasaki, T., 2006. Exfoliating layered double hydroxides in formamide: a method to obtain positively charged nanosheets. J. Mater. Chem. 16, 3809-3813.
Ookubo, A., Ooi, K. and Hayashi, H.,1993. Preparation and phosphate ion-exchange properties of a hydrotalcite-like compound. Langmuir 9(5), 1418-1422.
Pushparaj, S.S.C., Forano, C., Prevot, V., Lipton, A.S., Rees, G.J., Hanna, J.V., Nielsen, U.G., 2015. How the Method of Synthesis Governs the Local and Global Structure of Zinc Aluminum Layered Double Hydroxides. J. Phys. Chem. C 119, 27695-27707.
Staal, L.B., Pushparaj, S.S.C., Forano, C., Prevot, V., Ravnsbaek, D.B., Bjerring, M., Nielsen, U.G., 2017. Competitive reactions during synthesis of zinc aluminum layered double hydroxides by thermal hydrolysis of urea. J. Mater. Chem. A 5, 21795-21806.
Wang, L.J.,2010. Dihydrogen Phosphate Anion-Intercalated Layered Double Hydroxides: Synthesis and Selective IR Absorption Effect. Chinese Journal of Inorganic Chemistry 26(6), 970-976.
Wang, S.-L., Hua Liu, C., Kuang Wang, M., Hui Chuang, Y. and Chiang, P.-N. (2009) Arsenate adsorption by Mg/Al–NO3 layered double hydroxides with varying the Mg/Al ratio.
Wei, Y., Li, F., Liu, L., 2014. Liquid exfoliation of Zn–Al layered double hydroxide using NaOH/urea aqueous solution at low temperature. Rsc Adv. 4, 18044-18051.
Wu, Q., Olafsen, A., Vistad, Ø.B., Roots, J., Norby, P., 2005. Delamination and restacking of a layered double hydroxide with nitrate as counter anion. J. Mater. Chem. 15, 4695-4700.
Yang, K., Yan, L.G., Yang, Y.M., Yu, S.J., Shan, R.R., Yu, H.Q., Zhu, B.C., Du, B., 2014. Adsorptive removal of phosphate by Mg–Al and Zn–Al layered double hydroxides: Kinetics, isotherms and mechanisms. Sep. Purif. Technol. 124, 36-42.
Yu, J., Martin, B.R., Clearfield, A., Luo, Z., Sun, L., 2015. One-step direct synthesis of layered double hydroxide single-layer nanosheets. Nanoscale 7, 9448-9451.

Zhang, Y., Li, H., Du, N., Zhang, R. and Hou, W.,2016. Large-scale aqueous synthesis of layered double hydroxide single-layer nanosheets. Colloids and Surfaces A: Physicochemical and Engineering Aspects 501, 49-54.

Research Data Related to this Submission

There are no linked research data sets for this submission. The following reason is given:
Data will be made available on request

From: Corresponding Author

Prof. Gang Pan

Key Laboratory of Environmental Nanotechnology and Health Effects, Research Center for Eco-Environmental Sciences, Chinese Academy of Sciences, 18 Shuangqing Road, Beijing 100085, P. R. China

Centre of Integrated Water-Energy-Food Studies (*i*WEF), School of Animal, Rural and Environmental Sciences, Nottingham Trent University, Brackenhurst Campus, NG25 0QF, UK

E-mail: gpan@rcees.ac.cn

28-Jan-2019

Dear editor,

On behalf of my co-authors, I am submitting the revised manuscript entitled "Phosphate capture by ultrathin MgAl layered double hydroxide nanoparticles" (Manuscript ID: CLAY12322) by Chen Liu, Meiyi Zhang, Gang Pan, Laura Lundehøj, Ulla Gro Nielsen, Yi Shi, and Hans Christian Bruun Hanse. The itemized response to reviewer's comments is attached. We appreciate these comments very much, which are very helpful in improving the quality of the paper.

Thank you very much for your help.

Yours sincerely,

Gang Pan.

Reviewer(s)' Comments to Author:

Response to comments:

We have carefully revised the paper according to editor's and the reviewers' comments. The itemized responses to the comments are listed below.

Reviewer #1:

This manuscript describes phosphate ions capture by LDH powder consisting fine particles. It contains some useful information for readers of Applied Clay Science, but the following items must be considered before the publication. In addition, this manuscript is rather lengthy. The authors should revise the manuscript more concise.

1. Highlights and Abstract: In the experiment of this manuscript, the authors used LDH powder that is aggregation of fine LDH particles, not colloidal state of fine particle. "LDH nanoparticles exhibit" in Highlights and L26-27 in Abstract, these expressions may mislead readers into believing that colloidal LDHs were used. The authors should correct them.

   Response: 'LDH nanoparticles exhibit' has been revised to 'The freeze-dried LDHns-U25 nanoparticles exhibit' in both Highlights and Abstract (Line 31).

2. L36, L311-315: The authors claim LDHns-U25 reached equilibrium rapidly (within 15 min), compared with previous reports in the literature. However, usually ultrasonic treatment is not used before adsorption. The ultrasonic treatment may the cause for quick equilibrium. The authors should give result of kinetics about LDH-Ref, which was LDH prepared by conventional method. By comparison between results of LDHns-U25 and LDH-Ref, the authors can judge what is the cause for quick equilibrium. If the authors do not give the result of LDH-Ref about this, they should not claim quick equilibrium. They can just say that in this condition LDHns-25 reached equilibrium within 15 min in the result section, and cannot claim "fast" reaction in Abstract.

   Response: Ultrasonic treatment is usually used to minimize nanoparticle aggregation of LDH suspension (Fang et al. 2015, Zhang et al. 2016). Similar

treatment has also been used by magnetic nanoparticles in studies of adsorption of As(V) and As(III) (Cheng et al. 2015). Ultrasonic treatment alone cannot induce the delamination of conventional LDH. Only in the presence of an organic solvent or delaminating agent, for example formamide, can exfoliation take place (Ma et al. 2006, Wei et al. 2014, Wu et al. 2015). The fast adsorption has also been observed by adsortpion of As to ultrathin γ-Fe_2O_3 nanosheets (Liu et al. 2016), where the capture of As(III) and As(V) increases rapidly in the first 15 min and then plateaus for the next 6 hours. Hence, there is high possibility that the nano-structure and strong surface complexation between the nanoparticles and the phosphate ions are the reasons of fast adsorption (line 278-284).

3. L189-197, 198-200 & 211-213: In the experiment of adsorption, it is difficult to know the concentration of each element. For example, "using 1g L-1" does not mean the concentration of LDH in the finally adjusted solution: readers cannot calculate LDH concentration after the LDH suspension with concentration of 1g L-1 was mixed with unknown volumes of electrolyte and phosphate solution. The authors should clarify the concentration of LDH, phosphate and nitrate in the mixtures after mixing the suspension and solutions.

   Response: 30 mL was the total volume of electrolyte and phosphate solution. We added 30 mg LDH powder into the centrifuge tube, thus the LDH concentration in the suspension was 1g L^{-1}. To make this point clearer, we have rewritten the Phosphate adsorption section (section 2.4, line 153-181). Furthermore, to make the passage condense, “Experimental, 2.3 Solid State Characterization” has been shorten in manuscript and details can be found in Supporting Information (line 138-150, Supporting Information line 20-73).

4. L238: Fig 1b and Fig S1 may be the same one. If so, Fig. S1 is not necessary. In addition, "re-stacked" is not appropriate because LDH sheets were not stacked until dried. Like in the explanation for Fig S1, just "freeze-dried" is more appropriate.

Response: Fig. 1b shows the freeze-dried pristine LDH, while the previous Fig. S1 showed the freeze-dried LDH after phosphorus adsorption. Fig. S1 has been replaced by a combined figure showing XRD patterns of freeze dried MgAl-LDHs before and after phosphate adsorption. The data extracted from XRD characterization is shown in Table S1 (Supporting Information, line 76-80). "re-stacked" was deleted in the explanation for Fig. 1b (line 207).

5. L256: Mg/Al ratios of 1.97, 1.90 and 2.10 may be calculated from the result of ICP-OES, but it is not clear. Clarify this.

   Response: Yes, and the text has been clarified (Line 223-225).

6. L276: SEM images of LDH-Ref should be shown. In addition, Fig. S3 was not used in the text. Is Fig. S3 really necessary?

   Response: To make the manuscript more concise, we have moved the previous three SEM images to the Supporting Information and combined with the SEM images of LDH-Ref to produce a new Fig. S3 (Supporting Information, line 95-97).

7. L302-304: AFM images were provided only for LDHns-25. For comparison, at least AFM images of LDH-Ref should be provided. Crystallite size in the direction of 00l can be calculated from the result of Fig. 1b. The authors should compare the thickness values obtained from AFM with the above-mentioned crystallite sizes. In addition, what is "ScanAsyst mode"? It is not common word. Moreover, what is the difference between (a) and (b)?

   Response: AFM images of LDH-Ref has been shown in Fig. S4 (Supporting Information, line 98-102). For comparison, the AFM image of LDH-Ref along with the corresponding height profile is shown in Fig. S4. The size of LDH-Ref is

larger compared to LDH nanoparticles, with diameter of 100-150 nm and thickness of higher than 14 nm (line 268-271).

The thickness values obtained from AFM were compared with d_{003} in manuscript (Line 260-264). The d_{003} of LDHns-U25 is 0.817 nm (Table S1), which is close to the thickness of single metal hydroxide layer with interlayer (0.8 nm) (Yu et al., 2015). The AFM images reveals a particle thickness of 3 to 5 nm, containing four to six layers.

ScanAsyst mode is an image mode of AFM (Bruker). It is a PeakForce Tapping® based image optimization technique that enables every user to create the highest resolution AFM images using single-touch scanning (Supporting Information 55-57). One can visit the website 'https://www.bruker.com/products/surface-and-dimensional-analysis/atomic-force-microscopes/modes/modes/imaging-modes/scanasyst.html".

Fig.4 (a) and (b) are two views of LDHns-25, but with no big differences between them. Thus, we delete the previous Fig. 4(a) and combine the previous Fig.4(b) with Fig. 3 to produce Fig. 3(d) (line 254-258).

8. L330-331: In this part, do the authors mention contribution of adsorption on external surface of LDH particles? Do the authors also imply extra adsorption that does not come from exchange for interlayer anions? The sentence should be revised clearly.

   Response: we delete the puzzling sentence and discuss the adsorption mechanism in detail in the following sections.

9. L338-339: This sentence is puzzling.

   Response: The sentence has been revised to "Thus, desorption from LDH nanoparticles is low, hence increasing the potential of the LDH materials for water cleaning." (Line 306-308).

10. L 342: What does 73 to 42 mg g-1 refer to? In Fig 6b, data is expressed by %.

Response: We are sorry for the mistake in Fig. 6b, the unit should be mg g^{-1}. This has been revised in the manuscript (line 327).

11. L345-347: In this part, do the authors mention contribution of adsorption on external surface of LDH particles? The sentence should be revised clearly.

    Response: This refers to the adsorption on both external and internal surface of LDH particles.

12. L348-349: When pH increase, amount of OH- ions increase. Therefore, competition with OH- can be a cause for drop of phosphate adsorption too. The authors should consider this possibility.

    Response: The sentence has been revised to "Thus, the change in charge of phosphate ion, the LDH metal hydroxide layers and competition with OH- jointly cause adsorption to decrease with increasing pH. Furthermore, competition with carbonate is also more prevalent at high pH due to the unfavorable shift in the CO_2-equilibrium (Lundehøj et al, 2019)" (Line 317-320).

13. L377: It should be explained how to calculate contribution of AlOH.

    Response: We assign the broad resonance at $\delta_{iso}(^{31}P) \approx -9$ ppm to phosphate adsorbed to AOH and this P-AOH resonance constitute 6(4) to 12(6) % of the total P adsorbed, cf. Fig. 6. Thus, phosphate sorbed to the AOH component amounts to less than 15% of the sorption maximum (Line 344-353). The previous estimated calculation has been deleted.

14. L382: Why are not these resonances seen for the samples of this article?

    Response: We assign the broad resonance at $\delta_{iso}(^{31}P) \approx -9$ ppm to phosphate adsorbed to AOH and possibly a small amount of an amorphous aluminum phosphate ($AlPO_4$) phase based on our recent study of phosphate adsorption on ZnAl-LDH in acidified waste water sludge. We have revised the text and added an assignment based on our recent study of phosphate adsorption by ZnAl-LDH in

waste water (Lundehøj et al 2019)(Line 344-353). The text has been modified and our previous assignment based on earlier literature studies deleted.

15. L431: This sentence is puzzling. On L430-431, the authors seem to use the data of maximum adsorption amounts calculated from Langmuir equation. These maximum amounts includes adsorption on external surfaces, exchange for interlayer anions and adsorption to AlOH. Does "other mode" on L431 refer to anything other than these?

    Response: “other mode” refers to the mode that is different from electrostatic bonding. It could be exchange for interlayer anions, surface complexation, or adsorption on AOH. There was a mistake in line 402 and the sentence was revised to “A simple calculation accounting for the charge of the LDH interlayer and the charge of the phosphate anion provides an estimate of the maximum amount of phosphate (HPO_4^{2-}) that can be adsorbed due to electrostatic bonding (Supporting Information).” (Line 400-403).

16. L435-439: Discussion is not enough. The authors discuss contributions from each element: adsorption sites on external surface, exchange for interlayer anions and adsorption on AlOH. The authors should discuss the relationship among them. Especially, relationship between actual adsorption amounts and theoretical anion exchange capacities (AEC), which are proportional to Al amount (not maximum adsorption amounts calculated from Langmuir plot) should be discussed. When data in Tables 2 and 3 are compared, on the condition that phosphate ions are divalent, phosphate adsorption amounts are beyond AEC in the case of LDHns-F and LDHns-25. As for LDH-Res, the phosphate adsorption amounts was close to AEC. (Practical AEC will be equivalent to amount of nitrate ions in the interlayer space. Therefore, it is strongly recommended that the authors should provide data of nitrate contents in samples.) The authors should discuss relationship of the above-mentioned adsorption sites quantitively.

Response: We have measured nitrate content in the samples, but the values are not trustworthy due to long storage problem. We have estimate calculated the nitrate content based on the actual Mg and Al content in LDH samples. For LDHns-F and LDHns-U80, the theoretical AEC of LDH nanoparticles are close to adsorption capacities. For LDHns-U25, adsorption capacity from Langmuir fitting is 12% higher than calculated adsorption capacity. Since we do not have the AOH value for LDH-Ref, we use Mg and Al content from ICP-OES to calculate theoretical AEC, which is 40% higher than adsorption capacity. Wang et al. (2009) showed that Mg:Al ratio of 2:1 and 3:1 LDH have both vertical and horizontal orientations of interlayer nitrate ions. The interlayer nitrate with an orientation perpendicular to the hydroxide sheets can exchange with phosphate more readily while an orientation parallel to the sheets cannot. Hence only part of nitrate ions can be exchanged with phosphate.

Samples	Mg/Al in LDH	calculated AEC（mmol/g)	calculated adsorption capacity (mg P/g)	Langmuir fitting adsorption capacity (mg P/g)	Molecular formula
LDHns-F	2.63	3.05	94.7	89.6	$Mg_{2.63}Al(OH)_{7.25}NO_3^{-}2H_2O$
LDHns-U25	3.06	2.83	87.9	98.3	$Mg_{3.06}Al(OH)_{8.13}NO_3^{-}2H_2O$
LDHns-U80	2.50	3.13	96.9	97.6	$Mg_{3.06}Al(OH)_{7}NO_3^{-}2H_2O$
LDH-Ref	1.90	3.44	106.5	63.5	$Mg_{1.90}Al(OH)_{6}NO_3^{-}2H_2O$

17. L433 & 438: Does "surface" refer to external surface of LDH particles?

Response: ‘L433’: We cannot tell if the adsorption takes place on the external surface or internal surface based on ^{31}P MAS or both. There are few weak spinning side bands (Fig.6, line 355) but we cannot specify them (line 342-344).

‘L438’: Surface complexation refers to both internal and external surfaces of LDH nanoparticles.

18. L447: Data of Kuzawa et al. is missing in Table S4.

    Response: Added (Supporting Information, Table S4).

19. L451-452: In Table S4, data of Mg-Al LDHs other than those of this manuscript are not shown. Zn-LDH and Mg-Mn LDH are shown in Table S4, but Zn and Mn are heavy element. Therefore, adsorption amount per unit weight is unfair. The authors should compare the data of Mg-Al LDHs (e.g. 47.3 mg/g for granular HTAL (LDH content was ca. 90%) in Kuzawa, K. et al. (2006) Chemosphere 62, 45; 2.37mmol/g (73.4 mg/g) in Ookubo, A. at al. (1993) Langmuir 9, 1418) , and then claim whether the authors' sample show high adsorption ability or not. In addition, what does "high site density" exactly mean? Where are these sites? Explain clearly.

    Response: Zn-LDH and Mg-Mn LDH were deleted and Kuzawa et al. (2006), (Ookubo et al. 1993) were added in Table S4. The LDHns-U25 show higher adsorption capacities compared to granular HTAL, HTAL, Mg-Al LDH and MgAl-NO_3 LDH in the literature (Kuzawa et al. 2006, Ookubo et al. 1993, Yang et al. 2014, Khitous et al 2015) (Table S4, Supporting Information, line 111-114). "High site density" refers to a high density of adsorption sites that are not accessible in thicker LDH particles (line 428-429) (Fang et al, 2015).

20. L477: What is "coatings on porous host particles"? This is not explained in Results and Discussion section. In Conclusions section, the authors should not mention things that are not explained in the earlier sections.

    Response: This part has been deleted.

Reviewer #2:

Chen Liu et al present an interesting paper about the reactivity of ultrathin hydrotalcite LDH with phosphate. In fact, the initial product is a mixture of LDH and a significant amount of aluminum hydroxide gel that was detected with RMN. The authors provide an impressive amount of experimental data including XRD, TEM,

SEM, AFM, FTIR, surface potential measurements. The data are analyzed cautiously and the originality of the work is related to a relative increase of phosphate adsorption due to the special nature of the initial product. Due to the high quality of the data, the paper is suitable for publication in Applied Clay Science. However, some points are not completely clear and the paper could be improved by giving answers to the following questions:

> Main remarks:

1) Are you sure that the phosphate removal capacity are given in mg P-PO4 g-1 unit and not in mg7 PO4 g-1? I ask you this question because I am a bit surprised by some of the values provided for the "classical" hydrotalcite reference sample (synthesised by coprecipitation) and for ferrihydrite in Table S4.

   A P-PO4 removal capacity of 63,5 mg P-P04 g_1(classical hydrotalcite) would correspond to a PO4 removal capacity of about 190 mg PO4 g-1. This value is relatively high and I saw much lower values in literature data. Please provide also other values for classical hydrotalcite in Table S4. Same remarks for ferrihydrite, I am very surprised by the value of 77,2 mg P-PO4 that would correspond to a PO4 removal capacity of about 235 mg PO4 g-1. More recent references concerning ferrihydrite maximal values for ferrihydrite of about 80 mg P04 g-1 at pH of 7. Please check this important point in all the data given in the paper, e.g. page 4 the value of 45,9 mg g-1, is it P-PO4 or PO4?

   Response: Yes, the phosphate removal capacities are given in mg P g^{-1}, not mg PO_4 g^{-1} in this study. Same measures have been used for ferrihydrite and nano-$Mg(OH)_2$ in page 4. In Table S4, the values for granular HTAL, HTAL, MgAl-NO_3 LDH, CaAl-LDH, Phoslock, gibbsite, AOH, goethite, ferrihydrite, Fe-Al-Mn oxide are all given in mg P g^{-1}. The values for classical hydrotalcite are provided in Table S4 (Supporting Information, line 111-114).

2) The XRD data (modification of the c spacing or d003) should be more cautiously compared to literature data concerning the interaction of hydrotalcite with PO4. I

saw controversial data concerning the intercalation of PO4 into MgAl LDL. Some papers report some variation of the c spacing and other data do not. The variation of the d003 spacing should be discussed with more details in the paper. It seems that the ultrathin LDH present a initial c spacing different from the classical LDH. This may be discussed, is it due to the synthesis or is it due to a variation of the Mg-Al ratio. Ultrathin LDH seems to present a more opened initial structure that may incorporate more easily PO4.

Response: There is controversial data showing that d spacing decreased (from 8.37 Å to 7.61 Å) after phosphate adsorption on MgAl-NO_3 LDH and the paper claimed that this is because phosphate ion is smaller than nitrate (Khitous et al, 2015). However, more evidence in literature show intercalation of phosphate on colloidal MgAl-NO_3 LDH nanosheets (d_{003}=8.4 to 10.1 Å) (Koilraj et al. 2013), MgAl-CO_3 LDH (d_{003}=7.6 to 12.1 Å) (Wang et al. 2010), ZnAl-NO_3 LDH (d_{003}=8.8 to 11.1 Å) (He et al. 2010). Our data show a slight increase of d_{003} (LDH-Ref: d_{003}=7.77 to 8.11 Å; LDHns-U25: d_{003}=8.17 to 8.56 Å) after phosphate adsorption (see Figure below and Table S1). The little change in interlayer spacing after intercalation is in agreement with the findings in Gillman et al. (2008). This could be attributed to non-uniform distribution of phosphate/water in the interlayers (Gillman et al. 2008) (line 408-410). Wu et al. (2005) present a d_{003} value of 8.27 Å for classical MgAl-NO_3 LDH, which is higher than that of LDH-Ref but close to the d-spacing of LDH nanoparticles in our study.

3) Do you believe to the co-intecalation of PO4 and NO3 presented in the last figure of the paper or is it a simplified view. FTIR seems to indicate that NO3- is not fully replaced by PO4. A quantification of the quantity of NO3- species released in solution would give a more accurate answer to this question.

Response: In our study, $NaNO_3$ was added as electrolyte solution. The concentration of nitrate in the solution reduced from 10 to 3.4 mmol/l after phosphate adsorption. The concentration of nitrate added in the solution is much

higher than that of phosphate, thus competitive adsorption exists between nitrate and phosphates anions (line 395-399).

4) Page 13, a better explanation between the MgAl ratio "expected" and measured (Table 2) is missing. Is it the difference between the quantity introduced in the initial solution and the real value taking into account the presence of the Al hydroxide. I am not a specialist of NMR but how accurate are the quantitative estimation of Al hydroxide? The Al(OH)3 phase was not detected with other techniques, even with TEM, this is a bit surprising for a compound representing more than 10 % of the mixture.

Response: The relation between expected and measured Mg:Al ratios has been clarified (line 223-228). The initial Mg:Al ratios measured by ICP-OES are very close to the synthesis mixture (2:1). The real ratios take into account the presence of Al in AOH from ^{27}Al SSNMR (Table 2). The difference between the measured value and real value is because of the presence of AOH.

The $Al(OH)_3$/AOH (Amorphous aluminum hydroxide) phase is amorphous or poorly crystalline, hence it will not be detected by PXRD. Furthermore, the particle size is small so they are difficult to observe in TEM. ^{27}Al SSNMR is one of the most reliable methods for identification of AOH. The AOH concentrations above 3-5 % Al can be quantified by ^{27}Al SSNMR, as reported and discussed earlier by Nielsen and co-worked (Pushparaj et al. 2015, Staal et al. 2017).

5) You did not compare the kinetics data of ultrathin LDH with the reference classical LDH. Does the classical LDH adsorb PO4 also so quickly (15 min?). If not it should be mentioned.

Response: The phosphate adsorption on ultrathin LDHns-U25 is fast, compared to classical MgAl-LDH as reported in the literature, the equilibrium time will take from 40 min to a few hours(Das et al. 2006, Yang et al. 2014, Khitous et al. 2015) (Line 280-283).

> Minor remarks

> 1)line 48 "us" is "as"

> 2)space are missing lines 123, 133 and other problems with brakets

> 3) line 226 (001) is (003) ?

> 4) lines 230-231 sentence is unclear, please modify it. "ration" is "ratio".

Response: Revised (line 48, 123,132, 193, 197-200)

Reviewer #3:

1. I doubt the stability of LDH at pH 3.

   Response: The LDH is not stable at pH 3. In the pH effects experiment, we started at pH 7 to avoid the dissolution of LDH under 5 (Ookubo et al. 1993).

2. The PO4 loaded LDH may be characterized.

   Response: The phosphate loaded LDH was characterized by XRD (Supporting Information, Fig. S1, Table S1, line 76-80). Our data show a slight increase of d_{003} (LDH-Ref: d_{003}=7.77 to 8.11 Å; LDHns-U25: d_{003}=8.17 to 8.56 Å) after phosphate adsorption. The little change in interlayer spacing after intercalation is in agreement with the findings in Gillman et al. (2008). This could be attributed to non-uniform distribution of phosphate/water in the interlayers (Gillman et al. 2008) (line 408-410).

3. The following references may be referred in the introduction part of the manuscript.

> 1. Physico-Chemical Characterization and Adsorption Behaviour of Calcined Zn/Al Hydrotalcite- Like-Compound (HTlc) Towards Removal of Fluoride from Aqueous Solution. J. Coll. Interf. Sci. 261 (2003) 213-220.

> 2. Calcined Mg-Fe-CO3 layer double hydroxide as an adsorbent for the removal of selenite. J. Coll. Interf. Sci. 316 (2007) 216-223.

> 3. A Review on Recent Progress, Challenges and Perspective of Layered Double Hydroxides as Promising Photocatalysts, J. Mater. Chem. A,4 (2016), 10744-10766.

Response: Thank you for your recommendations. These references have been referred in the introduction part of the manuscript (line 57-58).

> Minor comments from the associate editor:

> - Correct terminology should be in agreement with the guide for authors, for instance abbreviations should not contain final 's' even in for plural in agreement with the guide for authors, please replace LDHs by LDH

Response: Checked

Reference

Cheng-Hua, L., Ya-Hui, C., Tsan-Yao, C., Yuan, T., Hui, L., Ming-Kuang, W. and Wei, Z.,2015. Mechanism of Arsenic Adsorption on Magnetite Nanoparticles from Water: Thermodynamic and Spectroscopic Studies. Environmental Science & Technology 49(13), 7726-7734.

Das, J., Patra, B.S., Baliarsingh, N., Parida, K.M., 2006. Adsorption of phosphate by layered double hydroxides in aqueous solutions. Appl. Clay Sci. 32, 252-260.

Fang, L., Huang, L., Holm, P.E., Yang, X., Hansen, H.C.B., Wang, D., 2015. Facile upscaled synthesis of layered iron oxide nanosheets and their application in phosphate removal. J. Mater. Chem. A 3, 7505-7512.

Gillman, G., Noble, M. and Raven, M.D.,2008. Anion substitution of nitrate-saturated layered double hydroxide of Mg and Al. Applied Clay Science 38(3-4), 179-186.

He, H., Kang, H., Ma, S., Bai, Y., Yang, X., 2010. High adsorption selectivity of ZnAl layered double hydroxides and the calcined materials toward phosphate. J. Colloid Interface Sci. 343, 225-231.

L. Lundehøj H.C. Jensen, L. Wybrandt, U. G. Nielsen, M.L. Christensen, C. A. Quist-Jensen., 2019. Layered Double Hydroxides for phosphorus recovery from

acidified and non-acidified dewatered sludge. Water Res. https://doi.org/10.1016/j.watres.2019.01.004

Khitous, M., Salem, Z. and Halliche, D.,2015. Removal of phosphate from industrial wastewater using uncalcined MgAl-NO3 layered double hydroxide: batch study and modeling. Desalination & Water Treatment 57(34), 1-12.

Koilraj, P., Antonyraj, C.A., Gupta, V., Reddy, C.R.K. and Kannan, S.,2013. Novel approach for selective phosphate removal using colloidal layered double hydroxide nanosheets and use of residue as fertilizer. Applied Clay Science 86(8), 111-118.

Liu, R., Liu, J.F., Zhang, L., Sun, J. and Jiang, G.,2016. Low Temperature Synthesized Ultrathin γ-Fe_2O_3 Nanosheets Show Similar Adsorption Behaviour for As(III) and As(V). Journal of Materials Chemistry A 4(20), 7606-7614.

Ma, R.Z., Liu, Z.P., Li, L., Iyi, N., Sasaki, T., 2006. Exfoliating layered double hydroxides in formamide: a method to obtain positively charged nanosheets. J. Mater. Chem. 16, 3809-3813.

Ookubo, A., Ooi, K. and Hayashi, H.,1993. Preparation and phosphate ion-exchange properties of a hydrotalcite-like compound. Langmuir 9(5), 1418-1422.

Pushparaj, S.S.C., Forano, C., Prevot, V., Lipton, A.S., Rees, G.J., Hanna, J.V., Nielsen, U.G., 2015. How the Method of Synthesis Governs the Local and Global Structure of Zinc Aluminum Layered Double Hydroxides. J. Phys. Chem. C 119, 27695-27707.

Staal, L.B., Pushparaj, S.S.C., Forano, C., Prevot, V., Ravnsbaek, D.B., Bjerring, M., Nielsen, U.G., 2017. Competitive reactions during synthesis of zinc aluminum layered double hydroxides by thermal hydrolysis of urea. J. Mater. Chem. A 5, 21795-21806.

Wang, L.J.,2010. Dihydrogen Phosphate Anion-Intercalated Layered Double Hydroxides: Synthesis and Selective IR Absorption Effect. Chinese Journal of

Inorganic Chemistry 26(6), 970-976.

Wang, S.-L., Hua Liu, C., Kuang Wang, M., Hui Chuang, Y. and Chiang, P.-N. (2009) Arsenate adsorption by Mg/Al–NO3 layered double hydroxides with varying the Mg/Al ratio.

Wei, Y., Li, F., Liu, L., 2014. Liquid exfoliation of Zn–Al layered double hydroxide using NaOH/urea aqueous solution at low temperature. Rsc Adv. 4, 18044-18051.

Wu, Q., Olafsen, A., Vistad, Ø.B., Roots, J., Norby, P., 2005. Delamination and restacking of a layered double hydroxide with nitrate as counter anion. J. Mater. Chem. 15, 4695-4700.

Yang, K., Yan, L.G., Yang, Y.M., Yu, S.J., Shan, R.R., Yu, H.Q., Zhu, B.C., Du, B., 2014. Adsorptive removal of phosphate by Mg–Al and Zn–Al layered double hydroxides: Kinetics, isotherms and mechanisms. Sep. Purif. Technol. 124, 36-42.

Yu, J., Martin, B.R., Clearfield, A., Luo, Z., Sun, L., 2015. One-step direct synthesis of layered double hydroxide single-layer nanosheets. Nanoscale 7, 9448-9451.

Zhang, Y., Li, H., Du, N., Zhang, R. and Hou, W.,2016. Large-scale aqueous synthesis of layered double hydroxide single-layer nanosheets. Colloids and Surfaces A: Physicochemical and Engineering Aspects 501, 49-54.

Phosphate capture by ultrathin MgAl layered double hydroxide nanoparticles

Chen Liu [a, c, g], Meiyi Zhang[*, a], Gang Pan[*, a, b, c], Laura Lundehøj [d], Ulla Gro Nielsen [d], Yi Shi [a, e] and Hans Christian Bruun Hansen [f, g]

[a] Research Center for Eco-Environmental Sciences, Chinese Academy of Sciences, Beijing 100085, China

[b] Center of Integrated Water-Energy-Food studies (iWEF), Nottingham Trent University, Nottinghamshire, NG25 0QF, UK

[c] University of Chinese Academy of Sciences, Beijing 100049, China

[d] Department of Physics, Chemistry and Pharmacy, University of Southern Denmark, Campusvej 55, 5230 Odense M, Denmark

[e] Shandong Key Laboratory of Water Pollution Control and Resource Reuse, School of Environmental Science and Engineering, Shandong University, Qingdao 266237, China

[f] Department of Plant and Environmental Sciences, University of Copenhagen, Thorvaldsensvej 40, DK-1871 Frederiksberg C, Denmark

[g] Sino-Danish Center for Education and Research (SDC), China

* Corresponding author: gpan@rcees.ac.cn (GP), myzhang@rcees.ac.cn

Abstract

Capture of phosphorus from runoff and wastewater is of high priority in order to reclaim phosphorus for food security and to prevent water pollution. Here we report an environmentally friendly method to synthesize ultrathin MgAl layered double hydroxide (LDH) nanoparticles for phosphorus adsorption. Fast co-precipitation of magnesium and aluminum at 25-80 °C in the presence of urea resulted in the desired LDH with variable admixtures of amorphous aluminum hydroxide (16-38%) quantified from solid state ^{27}Al MAS NMR. Freshly synthesized particles appeared as exfoliated single layers that upon drying stacked to form particles with thickness of 3 to 5 nm (four to six LDH layers) and lateral sizes of ~30 nm, as seen by XRD, SEM, TEM, and AFM. Phosphate adsorption on LDH nanoparticles synthesized at room temperature (LDHns-U25) was very fast and reaction reached equilibrium within 15 min at pH 8.5. The freeze-dried LDHns-U25 nanoparticles exhibited phosphate sorption capacity of 98±15 mg P g^{-1}, which is 55% higher than conventional LDH. Phosphate was bound to LDH electrostatically and via inner-sphere surface complexation as evidenced from a combination of ^{31}P MAS NMR spectroscopy, surface potential measurements, IR spectroscopy, and ionic strength effects on phosphate sorption. This study demonstrates that urea-facilitated synthesis of LDH nanoparticles provides fast and high capacity phosphate sorbents with potentials for phosphate recovery from waste waters.

Key words: Phosphate removal; Hydrotalcite-like compounds; Nanosheets; Adsorption; Wastewater

1. Introduction

Phosphorus is essential for agriculture and food security for the growing world population. However, excessive anthropogenic phosphate (P) arising from fertilization, treated municipal and industrial wastewater may cause eutrophication of receiving water bodies (Conley et al. 2009, Emmanuelawati et al. 2013, Shannon et al. 2008). Phosphorus capture and recycling is crucial, as phosphorus mineral deposits are being depleted (Pan et al. 2018, Reijnders 2014). Robust and efficient methods for P reduction at low cost and energy are therefore needed to address these challenges. Various technologies have been employed for phosphate removal from wastewaters, such as chemical precipitation, biological removal, ion exchange and adsorption. Among them, adsorption is promising due to less sludge production, high uptake capacity and efficiency at low P concentrations (Emmanuelawati et al. 2013, Moharami and Jalali 2013).

Layered double hydroxides (LDH) have been studied as sorbents for P removal due to their high anion-exchange capacity and their ability to accommodate different anions in the interlayer. LDH are layered structures comprising positively charged metal hydroxide layers typically comprising two different metal ions, interchanging with anionic interlayers of charge compensating anions (Das et al. 2003, Das et al. 2007, Mohapatra and Parida 2016). Here we refer to a specific LDH by the identity of the metal cations and the anion, e.g. MgAl-SO_4, for an LDH with magnesium and aluminum in the metal hydroxide layer and SO_4^{2-} in the interlayer. Promising P adsorption has been observed for MgAl-Cl, ZnAl-Cl, and ZnAl-NO_3 LDH from both synthetic solutions and waste waters (He et al. 2010, Kuzawa et al. 2006). New

generations of nanostructured adsorbents have been developed for P removal (Fang et al. 2015, Su et al. 2013) with high surface areas and abundant active adsorption sites. For instance, Zhang et al. (2015) reported a nano-$Mg(OH)_2$ modified polystyrene material exhibiting high adsorption capacity (45.6 mg P g^{-1}) for phosphate. However, the application of nanomaterials for wastewater cleaning has been challenged by complex manufacturing processes and use of toxic precursors.

Exfoliated LDH (here called LDH nanosheets) are interesting candidates as high capacity P adsorbents because they possess a permanent positive layer charge and a high specific surface area (Hibino and Jones 2001). A typical approach for formation of LDH nanosheets is to exfoliate pre-synthesized LDH layered compounds, usually by intercalation of large anionic solutes to weaken the interlayer interaction, followed by delamination of the modified products in organic solvents (Ma et al. 2006). However, the synthesis processes are time consuming and make use of costly (and toxic) organic solvents and reagents similar to other nano-adsorbents, which is a limitation for broader application.

In order to prevent stacking of the LDH nanosheets, one strategy is to introduce a stabilizer with high ability to form hydrogen bonds with hydroxyl groups as it may break the integrated bonding network among the hydroxyl groups of the metal hydroxide layers, the interlayer water molecules and anions (Wei et al. 2014). Formamide has been a classical agent for exfoliating LDH layers (Yu et al. 2015), but unfortunately makes synthesis unsustainable. Urea may represent a non-toxic alternative. The urea molecule has a high proportion of strongly electronegative

elements, one oxygen and two nitrogen atoms, implying a high capability of forming hydrogen bonds (Ma et al. 2006). Although homogeneous precipitation by thermal hydrolysis of urea - the so called 'urea method' (Costantino et al. 1998), results in LDH but with admixtures of amorphous Al-(hydr)oxide phases (Pushparaj et al. 2015), this method is frequently used for preparation of well-crystallized, large sized (2-20 μm) LDH under hydrothermal conditions (Adachi-Pagano et al. 2003, Hibino and Ohya 2009, Ogawa and Kaiho 2002). Progressive hydrolysis of urea usually produces hydroxide and carbonate ions, which are main components of the metal hydroxide layers and interlayers of LDH, and thus results in homogenous nucleation and crystallization of carbonate LDH (Hibino and Ohya 2009, Ogawa and Kaiho 2002) as well as formation of other layered phases (Staal et al. 2017). We hypothesize that a low reaction temperature may prevent urea hydrolysis, and thus that urea hydrates accumulate at the surface of LDH sheets, stabilizing the colloidal suspension, and causing the LDH layers to grow in-plane only and thus to produce LDH nanosheets.

In this study, we report a new route for directly synthesizing MgAl-NO_3 LDH nanosheet materials in urea solution. The P adsorption properties of this new material were studied with emphasis on adsorption kinetics, capacity and affinity as well as effects of solution pH and ionic strength. Solid state nuclear magnetic resonance (NMR) spectroscopy, zeta potential measurements, and Fourier transform infrared spectroscopy (FTIR) was used for characterization of the nanoparticles and P bonding.

2. Experimental

2.1 Materials

Magnesium nitrate ($Mg(NO_3)_2 \cdot 6H_2O$), aluminium nitrate ($Al(NO_3)_3 \cdot 9H_2O$), urea ($CO(NH_2)_2$), formamide (CH_3NO), concentrated nitric acid (HNO_3, 68 %), sodium hydroxide (NaOH, 98 %) and potassium dihydrogen phosphate (KH_2PO_4) were supplied by Sinopharm Chemical Reagent Co. (Beijing, China). All chemicals were of analytic grade (or higher), and was used without further purification. Deionized water was purged with high grade nitrogen (99.99%) for 30 min prior to use in order to remove carbon dioxide.

2.2 Synthesis of ultrathin LDH nanoparticles

Four different syntheses of MgAl-NO_3 LDH were performed in presence of urea at room temperature (LDHns-U25) and at 80°C (LDHns-U80), in formamide (LDHns-F), and by a conventional co-precipitation method (LDH-Ref), respectively. A 1 L solution containing $NaNO_3$ (0.01 M) and urea (6 M) was prepared in thermostatic water bath with pH adjusted to pH of 10.0 ± 0.5 using 0.5 M NaOH. A 200 mL mixed solution composed of 0.04 M $Al(NO_3)_3 \cdot 9H_2O$ and 0.08 M $Mg(NO_3)_2 \cdot 6H_2O$ was added dropwise (≈10-15 mL min^{-1}) to the beaker. Simultaneously, a solution of 0.5 M NaOH was added dropwise to maintain pH at 10.0 ± 0.5 under magnetic stirring (400 rpm) and N_2 flushing to avoid the entrance of CO_2 (30 mL min^{-1}) (Table 1). The pH was monitored using a Mettler Toledo combination pH electrode to ensure proper rate of NaOH addition. The resulting precipitate was collected by centrifugation for 15 min at 12840 g, washed twice with anhydrous ethanol and once with CO_2-free deionized water in sealed containers, and finally freeze-dried at -46°C for 24 h.

For comparison, LDHns-F was synthesized by modification of the method by Yu et al. (2015) using the same metal salt concentrations and the same reaction time as described above (Table 1). For reference, a conventional layered LDH-Ref was prepared using co-precipitation at constant pH similar to the method of Yun et al. (1995) (Table 1). The precipitate was stirred for 1 h and aged in water bath under stirring at 70°C for 24 h. All the other conditions were the same except formamide and urea was not added. The product was freeze-dried as described above.

Table 1. Composition of the solution, temperature and reaction time used for the synthesis of LDH.

2.3 Solid state characterization

The Mg and Al contents of the LDH samples were determined by inductively coupled plasma optical emission spectrometer (ICP-OES) and ^{27}Al magic angle spinning (MAS) NMR spectroscopy. The crystallinity, morphology and specific surface area of the LDHs synthesized were characterized by powder X-ray diffraction (XRD), field emission scanning electron microscopy (FESEM), transmission electronic microscopy (TEM), Atomic force microscopy (AFM), and Brunauer-Emmett-Teller N_2 adsorption (BET). A Zetasizer Nano ZS potential analyzer was used to measure the zeta potential of LDH particles in suspension before and after P adsorption. To study the phosphate speciation and bonding in the LDH, ^{31}P MAS NMR spectra and Transmission Fourier transform infrared spectroscopy (FTIR) were used. ^{27}Al MAS NMR spectroscopy was used to detect the presence of non-LDH impurities in the products, and to record LDH transformation when exposed to phosphate. Detailed

description of the measurements above can be found in the Supporting Information.

2.4 Phosphate adsorption

Phosphate adsorption kinetics was studied in batch experiments. Prior to use, the suspensions with a certain amount of freeze-dried LDH adsorbent dispersed in $NaNO_3$ electrolyte in polypropylene centrifuge tubes, were placed in an ultrasonic bath (80 kHz) for 30 min to minimize aggregation of LDH nanoparticles. Subsequently, various volumes of KH_2PO_4 solutions were added to the suspensions to yield a mixture volume of 30 mL, with LDH concentration of 1 g L^{-1} in 0.01 mol L^{-1} $NaNO_3$ background and different initial phosphate concentrations of 50 mg P L^{-1} and 80 mg P L^{-1}, respectively. The tubes were then shaken at 170 rpm for 8 h at 25±1°C, and the solution pH was kept constant at 8.5±0.1 using 0.1 M HNO_3/NaOH. The supernatant was separated by centrifugation after 3, 5, 7, 10, 15, 30, 60, 120, 240, 360, and 480 min at 12840 g for 5 min to determine the P concentration in the supernatants. The supernatants were filtered through a 0.22 μm polypropylene syringe filter and then analyzed for phosphate concentration using the molybdate colorimetric method at a wavelength of 880 nm using a spectrophotometer (UV-756 PC, Shanghai Sunny Hengping Scientific Instrument CO. LTD, China).

Adsorption isotherms were determined at pH 8.5±0.1 with the initial phosphate concentrations ranging from 10 to 120 mg P L^{-1} in presence of 1 g L^{-1} LDH and 0.01 M $NaNO_3$ electrolyte. The suspensions were constantly agitated for 24 h in a thermostatic shaker (25±1°C). After completion, suspensions were centrifuged, the supernatant sampled and the pellet re-dispersed in water to determine desorption of phosphate with

all experimental conditions maintained the same as during adsorption. Phosphate concentration was determined as described above. Adsorption data were fitted by the Langmuir isotherm model using non-linear regression in OriginPro 2016. The nitrate concentration of the solution after adsorption were measured by a colourimetric method (HACH, DR 1900).

In order to investigate how adsorption was affected by solution pH and ionic strength, 0.03 g freeze-dried LDH was added to 30 ml of 75 mg P L^{-1} solutions at three different electrolyte concentrations of 0.001, 0.01, or 0.1 M $NaNO_3$, respectively. The pH of the solution was adjusted from 7 to 11 using 0.1 M HNO_3/NaOH. After 24 h, the equilibrium pH was measured and the supernatants were filtered through 0.22 μm membrane for phosphate analysis.

3. Results and Discussion

3.1 Chemical and structural characterization of LDH nanoparticles

The phase composition of the synthesized freeze dried and gel-like fresh LDH was examined by powder-XRD (Fig. 1). When the freshly synthesized gel-like LDH product was examined, the basal reflections ((003) and (006)) were barely detectable (Fig. 1a), manifesting the lack of long-range order along the c-axis (Wang and O'Hare 2012, Yu et al. 2015). When samples were run as freeze-dried powder samples on a glass sample holder, a broad and intense basal reflection at 10.75° (0.82 nm) was observed demonstrating re-stacking of the colloidal LDH nanoparticles with nitrate in the interlayer (Fig. 1b) (Wu et al. 2005). The gel-like samples showed no signs of (003) basal reflections, but the characteristic (110) reflections was observed (Fig. 1a insert).

The cell parameter *a* (average metal-metal distance) calculated from the (110) reflection (X'Pert HighScore Plus) for dried LDHns-U25, LDHns-U80, LDHns-F and LDH-Ref samples were 3.054 Å, 3.048 Å, 3.048 Å and 3.045 Å, respectively. An *a* distance of 3.04 Å and 3.06 Å for Mg_2Al-NO_3 and Mg_3Al-NO_3 LDH, respectively have been observed by Hu1 and O'Hare (2005) and Wu et al. (2005), suggesting a Mg:Al ratio between 2:1 and 3:1 in our samples in agreement. Among the four samples, LDHns-U25 was synthesized at the lowest temperature, resulting in lowest intensity and broadest diffraction peaks (Fig. 1b). It can be concluded that direct synthesis in urea or formamide affords LDH nanoparticles with less crystallinity than that of traditional co-precipitation method.

Fig. 1. XRD patterns of (a) gel-like fresh sample of MgAl-LDH covered by Mylar film; inset: 110 reflection of gel-like fresh sample; (b) MgAl-LDH after freeze drying.

The purity of LDH preparations was further probed by ^{27}Al MAS NMR spectroscopy (Fig. 2). The asymmetric line shape of the isotropic resonance is characteristic for MgAl-LDH with impurities of amorphous aluminum hydroxides (AOH), see Pushparaj et al. (2015) and Staal et al. (2017) for a detailed discussion. Deconvolution of the ^{27}Al MAS NMR spectra allowed for an estimate of the relative concentration of the AOH phase admixture in the samples ranging between 16 and 38% (Fig. 2, Table S2). The admixture of AOH phases was expected given the fast metal salt addition, very short aging and absence of post synthesis treatment (Pushparaj et al. 2015). The relative AOH content was lower (16%) for the samples synthesized at 80°C

than for the samples prepared at 25°C (38%); hence the formation of AOH is temperature dependent, as observed earlier for co-precipitation (Pushparaj et al. 2015). In addition, all the samples contain less than 5% of tetrahedrally coordinated Al as seen from shifts at approx. 64 and 74 ppm, which most likely originates from a colloidal aluminum hydroxide gel (Staal et al. 2017).

The physiochemical properties of the LDH-Ref and the three LDH nanoparticle samples are summarized in Table 2. The bulk Mg:Al ratios of LDHns-F, LDHns-U25, LDHns-U80, and LDH-Ref samples were 1.97, 1.90, 2.10, and 1.91, respectively (calculated from ICP-OES), which are close to the Mg:Al ratios in the synthesis mixture. However, the actual Mg:Al ratios in LDH is higher (Table 2) because only 75±5 to 84±5 % of the total Al is in the LDH phase based on ^{27}Al SSNMR (Table S2), i.e., the LDH is depleted in Al as compared to the bulk composition (Staal et al. 2017) (see above). The N_2-adsorption/desorption isotherms of the LDH samples were analyzed to determine their specific surface areas and porosity (Fig. S2). The hysteresis loops display no limiting adsorption at high P/P_0, which is common for plate-like particles with slit-shaped pores (Zhan et al. 2016). All specific surface areas of the LDH nanoparticles (83-97 m^2 g^{-1}) were higher than that of LDH-Ref (52 m^2 g^{-1}, Table 2). The LDH samples display a distinct H3-type hysteresis loop (P/P_0 > 0.4), implying the presence of mesopores (2-50 nm). The average pore diameters of all the samples are small with a narrow distribution below 20 nm, indicating a mesoporous structure.

Fig. 2. Deconvolutions of the ^{27}Al MAS NMR spectra of the MgAl-LDH nanoparticles,

a) LDHns-F, b) LDHns-U80, c) LDHns-U25, d) LDHns-F_P, e) LDHns-U80_P and f) LDHns-U25_P. The experimental spectrum (Exp), simulated (Sim) and difference (Dif) are shown for each. The results are summarized in Table S2.

Table 2. Composition, BET and pore sizes of pristine LDH and nanoparticle samples

TEM images (Fig. 3) show that the three LDH samples synthesized in presence of formamide or urea have a sheet-like structure with a lateral size of ~30 nm, and a thickness of ~5 nm, respectively. The urea synthesis products are a few nanometers thick, evidenced by the slender dark colored area (Fig. 3a-b), where some of the particles are obviously curled. Sample LDHns-U25 (Fig. 3a) consists of very small, less well defined and highly aggregated particles which probably is due to a relatively high amount of AOH in this sample compared to its counterparts that were synthesized at 80°C (Table S2). The inset in Fig. 3c displays the basal plane of an individual LDH hexagon. The representative SEM images of the samples (Figure S3, Supporting Information) also confirm the formation of ultrathin sheet-like morphology.

Fig. 3. TEM images of LDH nanoparticles: a): LDHns-U25; b): LDHns-U80; c): LDHns-F; (d) AFM image and the corresponding height profile for the marked line in the image for LDHns-U25 mapped in ScanAsyst mode, height image over scanning area of 200×200 nm^2.

To further quantify the thickness of LDH nanoparticles, the freeze-dried materials were examined by AFM. The height profile along transects across particles are shown

in Fig. 3d, which reveals a particle thickness of 3 to 5 nm. Fig. 3d displays sheet-like objects with a similar lateral size as observed by TEM (Fig. 3c). The thickness for a single metal hydroxide layer with the interlayer is 0.8 nm as seen from XRD (Fig.1b). Particles with thicknesses of 3 to 5 nm thus consist of approximately four to six layers (Li et al. 2005, Ma et al. 2006). These compelling evidences confirm the formation of LDH nanoparticles with a thickness of only few layers consistent with previous studies of exfoliated layered LDH (Fang et al. 2015, Hibino and Jones 2001, Ma et al. 2006). For comparison, the AFM image of LDH-Ref along with the corresponding height profile is shown in Fig. S4. The size of LDH-Ref is larger compared to LDH nanoparticles, with diameter of 100-150 nm and thickness of higher than 14 nm. This may due to long crystallization time of the synthesis process.

3.2 Phosphate adsorption

The kinetics of phosphate adsorption to LDHns-U25 at different initial phosphate concentrations were well fitted by a pseudo second-order model (eqn. (1)) (Fig. 4a, parameters in Table S3).

$$\frac{t}{q_t} = \frac{1}{k_2 q_e^2} + \frac{1}{q_e} t \qquad (1)$$

where q_t is the adsorbed amount at a time t (mg g^{-1}), q_e is the adsorbed amount at equilibrium, and k_2 (g mg^{-1} min^{-1}) the rate constant. Phosphate adsorption occurred rapidly and reached equilibrium within 15 min. Similar fast adsorption (within 15 min) has been observed by ultrathin γ-Fe_2O_3 nanosheets (Liu et al. 2016). Phosphate adsorption to LDHns-U25 is fast, compared to many other layered MgAl-LDH, which the equilibrium time will take from 40 min to a few hours (Das et al. 2006, Yang et al.

2014, Khitous, M. et al. 2015). For metal oxides, the equilibrium time will be several hours (Ren et al. 2012, Yu and Chen 2015).

Fig. 4. a) Kinetics of phosphate adsorption to LDHns-U25 and corresponding pseudo-second-order kinetics (eqn(1)); b) Adsorption isotherms for phosphate adsorption to pristine LDH and LDH nanoparticles and the corresponding Langmuir fits (error bars represent the standard deviation of duplicates).

Table 3. Langmuir isotherm parameters of the LDH.

Isotherm data were well described by the Langmuir model (eqn(2)) (Fig. 4b, Table 3).

$$q_e = \frac{K_L C_e q_m}{1+K_L C_e} \qquad (2)$$

where C_e (mg P L^{-1}) is the equilibrium phosphate concentration in solution, q_e (mg P g^{-1}) the amount of phosphate adsorbed, q_m (mg P g^{-1}) the maximum adsorption capacity, and K_L (L mg(P)$^{-1}$) the Langmuir affinity constant. The maximum phosphate adsorption capacity obtained from Langmuir fitting follows this sequence: LDHns-U25 > LDHns-F > LDHns-U80 > LDH-Ref, with q_m spanning from 98.3±14.6 mg P g^{-1} to 63.5±8.6 mg P g^{-1}. Desorption of phosphate from the phosphate loaded nanoparticles was evaluated after adsorption experiments by replacement of the solution with fresh electrolyte without phosphate, and controlling pH at 8.5. The extent of phosphate desorption was calculated by dividing the desorbed amount after 24 h by the initial adsorbed amount. Phosphate desorption from LDHns-U25 and LDHns-U80 were low, with the lowest values of 0.17±0.03% and 0.82±0.04% at low P loadings, and

the highest of 5.04±0.28% and 6.23±0.21% at high P loadings (Fig. 5a). Thus, desorption from LDH nanoparticles is low, hence increasing the potential of the LDH materials for water cleaning.

Fig. 5b reveals the effects of pH and ionic strength on phosphate adsorption by LDHns-U25. In the studied pH range 7-11, phosphate adsorption dropped significantly from ~73 to ~42 mg g^{-1} with increasing pH. Similar solution pH effect on phosphate adsorption has also been observed for Mg-Al LDH (Yang et al. 2014). The protonation of the hydroxyl groups of the MgAl hydroxide layers will change with pH contributing with positive surface charge at low pH and negative surface charge at high pH. At higher pH, LDH layers become increasingly deprotonated and causes electrostatic repulsion between phosphate and deprotonated surface OH groups (Chitrakar et al. 2006). Thus, the change in charge of phosphate ion, the change in charge of the LDH metal hydroxide layers and competition with OH^- jointly cause adsorption to decrease with increasing pH. Furthermore, competition with carbonate is also more prevalent at high pH due to the unfavorable shift in the CO_2-equilibrium (Lundehøj et al, 2019).

Increasing the ionic strength from 0.001 M to 0.1 M had no significant effect on adsorption (Fig. 5b). This is a strong indication that adsorption may take place via inner-sphere surface complexation (McBride 1997, Su et al. 2013, Zhang et al. 2009) which is insensitive to ionic strength as opposed to outer-sphere surface complexation that decreases with increasing ionic strength (Su et al. 2013). Thus, the results suggest that phosphate form inner-sphere complexes when adsorbed on LDH nanoparticles.

Fig. 5. (a) Phosphate desorption from LDH nanoparticles (pH 8.5±0.1, desorption time: 24 h); (b) The effect of pH and ionic strength on phosphate adsorption by LDHns-U25 (error bars represent the standard deviation of duplicates).

3.3 Phosphate bonding to LDH nanoparticles

3.3.1 Solid state NMR

^{27}Al MAS NMR spectra of LDH nanoparticles were recorded after exposure to phosphate. The deconvolutions of these spectra showed no significant changes in the relative concentration for the LDH component, indicating that the LDH is not dissolved or transformed when exposed to phosphate. ^{27}Al MAS NMR spectra of the LDH nanoparticles after phosphate adsorption showed a small (0.5-0.7 ppm) change in δ_{iso} (^{27}Al) indicating incorporation of phosphate in the interlayer of the LDH. ^{31}P MAS NMR spectra were used to study phosphate speciation and bonding in the LDH. The ^{31}P MAS NMR spectra contain one resonance, accompanied by a few weak spinning side bands (Table 4, Fig. 6). These results are in good agreement with earlier studies on MgAl-LDH (Hou et al. 2003). The presence of multiple ^{31}P sites imply that in addition to electrostatic bonding in their interlayer, phosphate may also form surface complexes on e.g., the edges and outside of the particles. In addition, phosphate also sorb to AOH present in the LDH nanoparticle samples according to ^{27}Al SSNMR (Table S2); We assign the broad resonance at δ_{iso}(^{31}P) ≈ -9 ppm to phosphate adsorbed to AOH and possibly a small amount of an amorphous aluminum phosphate ($AlPO_4$) phase based on our recent study of phosphate adsorption on ZnAl-LDH in acidified waste water sludge (Lundehøj et al 2019). We note that the

^{27}Al SSNMR spectra of the P-loaded samples have a small intensity (< 5 %) in the region 0 to -5 ppm for $AlPO_4$, but could not be determined precisely from deconvolution. This P-AOH resonance constitute 6(4) to 12(6) % of the total P c.f., Figure 6. Thus, phosphate sorbed to the AOH component is less than 15% of the sorption maximum.

Table 4. Parameters obtained from the deconvolutions of the ^{31}P MAS NMR spectra

Fig. 6. Deconvolution of the experimental ^{31}P MAS NMR spectra of the MgAl-LDH nanosheets exposed to phosphate. a) LDHns-F_P, b) LDHns-U80_P, and c) LDHns-U25_P. The experimental spectrum (Exp), simulated (Sim) and difference (Dif) are shown for each.

3.3.2 Surface zeta potentials

Fig. 7a shows the zeta potentials of pure LDH nanoparticles before and after exposure to 50 mg P L^{-1} phosphate solution. Before the adsorption, the surface charge of LDH nanoparticles is positive in the studied pH range, but a decline is seen with increasing pH as the surface OH groups are increasingly deprotonated (Hansen and Koch 1995). After phosphate adsorption, the surface charge of LDH nanoparticles decreased significantly, and the isoelectric point of LDHns-U25 and LDHns-U80 was determined to pH 5.3 and 5.7, respectively. The marked decrease of the zeta potential after phosphate adsorption indicates that phosphate adsorbed to LDH nanosheet surfaces is bound as inner-sphere surface complexes as formation of outer-sphere surface complexes cannot shift the surface charge of this magnitude (Ren et al. 2012, Su

et al. 2013, Yang et al. 2014).

Fig. 7. a) Zeta potential of LDHns-U25 and LDHns-U80 before (solid line) and after (dot line) phosphate adsorption with initial phosphate concentration of 50 mg L^{-1}, adsorbent dose at 1g L^{-1}; b) FT-IR spectra of LDHns-U25 before (A) and after (B_{1-4}) phosphate adsorption at different phosphate initial concentrations: B_1= 20 mg L^{-1}, B_2= 50 mg L^{-1}, B_3= 80 mg L^{-1}, B_4= 120 mg L^{-1}.

3.3.3 FT-IR analysis

The FT-IR spectrum of non-treated LDHns-U25 is compared with the P-loaded sorbents at several different initial P concentrations (Fig. 7b). The strong and broad bands at 3453 cm^{-1} and 1632 cm^{-1} belong to the stretching and bending vibration of the hydroxyl groups (–OH) in the LDH metal hydroxide layers and water, respectively (Liu et al. 2010, Zhang et al. 2005). The bands at ca.1384 cm^{-1} are identified as υ_3 mode of NO_3^- (Wu et al. 2005) in the interlayer. The hydrolysis of urea proceeds in two steps, with first formation of NH_4CNO (2200 cm^{-1}) and next formation of ammonium and carbonate (Adachi-Pagano et al. 2003). However, none of these bands were observed in the IR spectra demonstrating that urea was not decomposed during synthesis (Benito et al. 2008). After reaction with phosphate solution, a new, broad band at 1059-1067 cm^{-1} appeared, which can be assigned to the symmetrical stretching vibration of phosphate (Yu and Chen 2015). Its intensity increased with the phosphate concentration used indicating that the surface hydroxyl groups were replaced by the adsorbed phosphate via formation of an inner-sphere surface complex (M-O-P) between phosphate and the

LDH metal hydroxide layers (Lǔ et al. 2013, Yu and Chen 2015, Zhan et al. 2016), in accordance with the results of ionic strength and zeta potential measurements. The 1384 cm^{-1} peak (NO_3^-) decreased with increasing phosphate concentration, in accordance with decreasing nitrate concentration from 10 to 3.4 mmol l^{-1} after adsorption, suggesting that competitive adsorption exists between phosphate anions and nitrate in the solution. This could be attributed to much higher concentration of $NaNO_3$ electrolyte than phosphate in the solution.

A simple calculation accounting for the charge of the LDH interlayer and the charge of the phosphate anion provides an estimate of the maximum amount of phosphate (HPO_4^{2-}) that can be adsorbed due to electrostatic bonding (Supporting Information). The estimated amounts represent 50-70% of the maximum P adsorption capacity. Thus, other modes of adsorption than electrostatic bonding are active. The observation of four different environments in the ^{31}P NMR spectra support the adsorption on the surface of the particles and intercalation of P in the interlayer. The latter was also confirmed by a slight increase of d-spacing after P adsorption (Fig. S1, Table S1) (Hansen 1995). The little change in interlayer spacing after intercalation is in agreement with the findings in Gillman et al. (2008). This could be attributed to non-uniform distribution of phosphate/water in the interlayers (Gillman et al. 2008). The adsorption mechanism on LDH can be speculated as illustrated in Fig.8: there was electrostatic attraction between negatively charged phosphate species and positively charged LDH nanoparticles; inner-sphere surface complexation may be formed when phosphate was adsorbed on the surface of the LDH nanoparticles; ion exchange

between phosphate anions and interlayer NO_3^-.

Fig. 8. The possible synthesis process and P adsorption mechanisms by LDH nanoparticles（Yang et al. 2014）.

3.4 Perspectives for applications

Table S4 compares the maximum adsorption capacities of various adsorbents for phosphate. It is found that the LDH nanoparticles produced in this work have a significantly higher phosphate removal capacity than many other adsorbents, e.g. granular MgAl LDH (hydrotalcite) (Kuzawa et al. 2006), hydrotalcite (Ookubo at al. 1993), MgAl LDH (Yang et al. 2014), gibbsite (Lookman et al. 1997), goethite (Kim et al. 2011), and phoslock, a commercial lanthanum exchanged bentonite which is used for trapping P in lake restauration (Robb et al. 2003, Ross et al. 2008, Spears et al. 2013, Xu et al. 2017). A high adsorption capacity of our LDH nanoparticles compared to other layered LDH may be attributed to the thin particles contributing a high density of adsorption sites that are not accessible in thicker LDH particles (Fang et al. 2015). The remarkably high adsorption capacity of 131 mg P g^{-1} for CaAl LDH (hydrocalumite) is due to precipitation of calcium phosphates as the LDH dissolves (Xu et al. 2010). Amorphous aluminum hydroxide which is present in our samples (Fig. S4) has an adsorption capacity less than half of that for LDHns-U25. Many adsorbents including iron oxides (Lǔ et al. 2013, Zhang et al. 2009) and zirconium oxides (Su et al. 2013) often have negative surface charges at the pH of natural waters and thus sorption may be rather low even at pH 7 (Xu et al. 2017). On the contrary, LDH nanoparticles

can be used even at high pH which may be encountered during eutrophication events such as cyanobacterial blooms (pH～8.5).

4. Conclusion

This study presents a facile method for the synthesis of Mg-Al LDH nanoparticles using urea as a dispersing agent to limit layer stacking. The mesoporous material consists of platy particles with a thickness of 3-5 nm and diameters of approximately 30 nm contributing to a specific surface area of 84 m^2 g^{-1}. The freshly synthesized and non-aged products contain variable amounts of admixed AOH (16-38%). The LDH nanoparticles show very fast (15 min) phosphate adsorption and a high phosphate adsorption capacity of close to 100 mg P g^{-1} at pH 8.5. The ^{31}P MAS NMR spectroscopy showed that phosphate adsorption occurs by intercalation in the interlayer (ion exchange) and inner-sphere surface complexation. The latter was confirmed by ionic strength effects on adsorption, zeta-potential measurements and IR spectroscopy. NMR showed the LDH to be stable during phosphate adsorption and less than 7% of adsorbed P desorbed on 24 h desorption tests. Easy, cheap and environmentally friendly synthesis, fast and high capacity adsorption even for high pH waters and low phosphate desorption makes the new LDH adsorbent interesting for treatment of waste waters or phosphate rich runoff.

Acknowledgements

This work was financially supported by National Key R&D Program of China [grant numbers 2017YFA0207204], and National Natural Science Foundation of China [grant numbers 21377003], the Villum Foundation via the “Villum Young Investigator

Programme" [grant numbers VKR022364] (UGN, LL), the Innovation Foundation, Denmark (ReCoverP), Sino-Danish Center and Beijing Natural Science Foundation [grant numbers 8162040].

References

Adachi-Pagano, M., Forano, C., Besse, J.-P., 2003. Synthesis of Al-rich hydrotalcite-like compounds by using the urea hydrolysis reaction-control of size and morphology. J. Mater. Chem. 13, 1988-1993.

Benito, P., Herrero, M., Barriga, C., Labajos, F.M., Rives, V., 2008. Microwave-assisted homogeneous precipitation of hydrotalcites by urea hydrolysis. Inorg. Chem. 47, 5453-5463.

Chitrakar, R., Tezuka, S., Sonoda, A., Sakane, K., Ooi, K., Hirotsu, T., 2006. Selective adsorption of phosphate from seawater and wastewater by amorphous zirconium hydroxide. J. Colloid Interface Sci. 297, 426-433.

Conley, D.J., Paerl, H.W., Howarth, R.W., Boesch, D.F., Seitzinger, S.P., Havens, K.E., Lancelot, C., Likens, G.E., 2009. Controlling eutrophication: nitrogen and phosphorus. Science 323, 1014-1015.

Costantino, U., Marmottini, F., Nocchetti, M., Vivani, R., 1998. New synthetic routes to hydrotalcite-like compounds-characterisation and properties of the obtained materials. Berichte Der Deutschen Chemischen Gesellschaft, 1439-1446.

Das, D.P., Das, J. and Parida, K.,2003. Physicochemical characterization and adsorption behavior of calcined Zn/Al hydrotalcite-like compound (HTlc) towards removal of fluoride from aqueous solution. J. Colloid Interface Sci.

261(2), 213-220.

Das, J., Patra, B.S., Baliarsingh, N., Parida, K.M., 2006. Adsorption of phosphate by layered double hydroxides in aqueous solutions. Appl. Clay Sci. 32, 252-260.

Das, J., Patra, B.S., Baliarsingh, N., Parida, K.M., 2007. Calcined Mg-Fe-CO_3 layer double hydroxide as an adsorbent for the removal of selenite. J. Colloid Interface Sci. 316, 216-223.

Emmanuelawati, I., Yang, J., Zhang, J., Zhang, H.W., Zhou, L., Yu, C.Z., 2013. Low-cost and large-scale synthesis of functional porous materials for phosphate removal with high performance. Nanoscale 5, 6173-6180.

Fang, L., Huang, L., Holm, P.E., Yang, X., Hansen, H.C.B., Wang, D., 2015. Facile upscaled synthesis of layered iron oxide nanosheets and their application in phosphate removal. J. Mater. Chem. A 3, 7505-7512.

Gillman, G., Noble, M. and Raven, M.D.,2008. Anion substitution of nitrate-saturated layered double hydroxide of Mg and Al. Applied Clay Science 38(3-4), 179-186.

Hansen, H.C.B., 1995. Interlayer bonding of orthophosphate and orthosilicate in layered magnesium-aluminium hydroxide (hydrotalcite), International Clay Conference, pp. 201-206.

Hansen, H.C.B., Koch, C.B., 1995. Synthesis and characterization of pyroaurite. Appl. Clay Sci. 10, 5-19.

He, H., Kang, H., Ma, S., Bai, Y., Yang, X., 2010. High adsorption selectivity of ZnAl layered double hydroxides and the calcined materials toward phosphate. J. Colloid Interface Sci. 343, 225-231.

Hibino, T., Jones, W., 2001. New approach to the delamination of layered double hydroxides. J. Mater. Chem. 11, 1321-1323.

Hibino, T., Ohya, H., 2009. Synthesis of crystalline layered double hydroxides: Precipitation by using urea hydrolysis and subsequent hydrothermal reactions in aqueous solutions. Appl. Clay Sci. 45, 123-132.

Hou, X., Bish, D.L., Wang, S.L., Johnston, C.T., Kirkpatrick, R.J., 2003. Hydration, expansion, structure, and dynamics of layered double hydroxides. Am. Mineral. 88, 167-179.

Hu, G., O'Hare, D., 2005. Unique layered double hydroxide morphologies using reverse microemulsion synthesis. J. Am. Chem. Soc., 17808-17813.

Khitous, M., Salem, Z. and Halliche, D.,2015. Removal of phosphate from industrial wastewater using uncalcined MgAl-NO_3 layered double hydroxide: batch study and modeling. Desalination & Water Treatment 57, 1-12.

Kim, J., Li, W., Philips, B.L., Grey, C.P., 2011. Phosphate adsorption on the iron oxyhydroxides goethite (α-FeOOH), akaganeite (β-FeOOH), and lepidocrocite (γ-FeOOH): a ^{31}P NMR Study. Energy Environ. Sci. 4, 4298-4305.

Kuzawa, K., Jung, Y.J., Kiso, Y., Yamada, T., Nagai, M., Lee, T.G., 2006. Phosphate removal and recovery with a synthetic hydrotalcite as an adsorbent. Chemosphere 62, 45-52.

Li, L., Ma, R., Ebina, Y., Nobuo Iyi, A., Sasaki, T., 2005. Positively charged nanosheets derived via total delamination of layered double hydroxides. Chem. Mater. 17, 4386-4391.

Liu, H., Deng, S., Li, Z., Yu, G., Huang, J., 2010. Preparation of Al–Ce hybrid adsorbent and its application for defluoridation of drinking water. J. Hazard. Mater. 179, 424-430.

Liu, R., Liu, J.F., Zhang, L., Sun, J. and Jiang, G.,2016. Low temperature synthesized ultrathin γ-Fe_2O_3 nanosheets show similar adsorption behavior for As(III) and As(V). J. Mater. Chem. A 4, 7606-7614.

Lookman, R., Grobet, P., Merckx, R., Van Riemsdijk, W.H., 1997. Application of ^{31}P and ^{27}Al MAS NMR for phosphate speciation studies in soil and aluminium hydroxides: promises and constraints. Geoderma 80, 369-388.

Lǔ, J., Liu, H., Liu, R., Zhao, X., Sun, L., Qu, J., 2013. Adsorptive removal of phosphate by a nanostructured Fe–Al–Mn trimetal oxide adsorbent. Powder Technol. 233, 146-154.

L. Lundehøj H.C. Jensen, L. Wybrandt, U. G. Nielsen, M.L. Christensen, C. A. Quist-Jensen., 2019. Layered double hydroxides for phosphorus recovery from acidified and non-acidified dewatered sludge. Water Res. https://doi.org/10.1016/j.watres. 2019.01.004

Ma, R.Z., Liu, Z.P., Li, L., Iyi, N., Sasaki, T., 2006. Exfoliating layered double hydroxides in formamide: a method to obtain positively charged nanosheets. J. Mater. Chem. 16, 3809-3813.

McBride, M.B., 1997. A critique of diffuse double layer models applied to colloid and surface chemistry. Clays Clay Miner. 45, 598-608.

Mohapatra, L. and Parida, K.,2016. A review on recent progress, challenges and perspective of layered double hydroxides as promising photocatalysts. J. Mater.

Chem. A 4, 10744-10766.

Moharami, S., Jalali, M., 2013. Removal of phosphorus from aqueous solution by Iranian natural adsorbents. Chem. Eng. J. 223, 328-339.

Ogawa, M., Kaiho, H., 2002. Homogeneous precipitation of uniform hydrotalcite particles. Langmuir 18, 4240-4242.

Ookubo, A., Ooi, K. and Hayashi, H.,1993. Preparation and phosphate ion-exchange properties of a hydrotalcite-like compound. Langmuir 9, 1418-1422.

Pan, G., Lyu, T., Mortimer, R.J., 2018. Closing phosphorus cycle from natural waters: re-capturing phosphorus through an integrated water-energy-food strategy. J. Environ. Sci. 65, 375-376.

Pushparaj, S.S.C., Forano, C., Prevot, V., Lipton, A.S., Rees, G.J., Hanna, J.V., Nielsen, U.G., 2015. How the method of synthesis governs the local and global structure of zinc aluminum layered double hydroxides. J. Phys. Chem. C 119, 27695-27707.

Reijnders, L., 2014. Phosphorus resources, their depletion and conservation, a review. Resour. Conserv. Recycl. 93, 32-49.

Ren, Z., Shao, L., Zhang, G., 2012. Adsorption of phosphate from aqueous solution using an Iron–Zirconium binary oxide sorbent. Water, Air, Soil Pollut. 223, 4221-4231.

Robb, M., Greenop, B., Goss, Z., Douglas, G., Adeney, J., 2003. Application of Phoslock (TM), an innovative phosphorus binding clay, to two Western Australian waterways: preliminary findings. Hydrobiologia 494, 237-243.

Ross, G., Haghseresht, F., Cloete, T.E., 2008. The effect of pH and anoxia on the performance of Phoslock® , a phosphorus binding clay. Harmful Algae 7, 545-550.

Shannon, M.A., Bohn, P.W., Elimelech, M., Georgiadis, J.G., Marinas, B.J., Mayes, A.M., 2008. Science and technology for water purification in the coming decades. Nature 452, 301-310.

Spears, B.M., Lurling, M., Yasseri, S., Castro-Castellon, A.T., Gibbs, M., Meis, S., McDonald, C., McIntosh, J., Sleep, D., Van Oosterhout, F., 2013. Lake responses following lanthanum-modified bentonite clay (Phoslock) application: an analysis of water column lanthanum data from 16 case study lakes. Water Res. 47, 5930-5942.

Staal, L.B., Pushparaj, S.S.C., Forano, C., Prevot, V., Ravnsbaek, D.B., Bjerring, M., Nielsen, U.G., 2017. Competitive reactions during synthesis of zinc aluminum layered double hydroxides by thermal hydrolysis of urea. J. Mater. Chem. A 5, 21795-21806.

Su, Y., Cui, H., Li, Q., Gao, S., Shang, J.K., 2013. Strong adsorption of phosphate by amorphous zirconium oxide nanoparticles. Water Res. 47, 5018-5026.

Wang, Q., O'Hare, D., 2012. Recent advances in the synthesis and application of layered double hydroxide (LDH) nanosheets. Chem. Rev. 112, 4124-4155.

Wei, Y., Li, F., Liu, L., 2014. Liquid exfoliation of Zn–Al layered double hydroxide using NaOH/urea aqueous solution at low temperature. Rsc Adv. 4, 18044-18051.

Wu, Q., Olafsen, A., Vistad, Ø.B., Roots, J., Norby, P., 2005. Delamination and restacking of a layered double hydroxide with nitrate as counter anion. J. Mater. Chem. 15, 4695-4700.

Xu, R., Zhang, M., Mortimer, R.J., Pan, G., 2017. Enhanced Phosphorus Locking by Novel Lanthanum/Aluminum-Hydroxide Composite: Implications for Eutrophication Control. Environ. Sci. Technol. 51, 3418-3425.

Xu, Y., Dai, Y., Zhou, J., Xu, Z.P., Qian, G., Lu, G.Q.M., 2010. Removal efficiency of arsenate and phosphate from aqueous solution using layered double hydroxide materials: intercalation vs. precipitation. J. Mater. Chem. 20, 4684-4691.

Yang, K., Yan, L.G., Yang, Y.M., Yu, S.J., Shan, R.R., Yu, H.Q., Zhu, B.C., Du, B., 2014. Adsorptive removal of phosphate by Mg–Al and Zn–Al layered double hydroxides: Kinetics, isotherms and mechanisms. Sep. Purif. Technol. 124, 36-42.

Yu, J., Martin, B.R., Clearfield, A., Luo, Z., Sun, L., 2015. One-step direct synthesis of layered double hydroxide single-layer nanosheets. Nanoscale 7, 9448-9451.

Yu, Y., Chen, J.P., 2015. Key factors for optimum performance in phosphate removal from contaminated water by a Fe-Mg-La tri-metal composite sorbent. J. Colloid Interface Sci. 445, 303-311.

Zhan, T., Zhang, Y., Yang, Q., Deng, H., Xu, J., Hou, W., 2016. Ultrathin layered double hydroxide nanosheets prepared from a water-in-ionic liquid surfactant-free microemulsion for phosphate removal from aquatic systems. Chem. Eng. J. 302, 459-465.

Zhang, G., Liu, H., Liu, R., Qu, J., 2009. Removal of phosphate from water by a Fe-Mn binary oxide adsorbent. J. Colloid Interface Sci. 335, 168-174.

Zhang, Q., Zhang, Z., Teng, J., Huang, H., Peng, Q., Jiao, T., Hou, L., Li, B., 2015. Highly efficient phosphate sequestration in aqueous solutions using nanomagnesium hydroxide modified polystyrene materials. Ind. Eng. Chem. Res. 54, 2940–2949.

Zhang, Y., Yang, M., Dou, X, He, H., Wang, D., 2005. Arsenate adsorption on an Fe−Ce bimetal oxide adsorbent: role of surface properties. Environ. Sci. Technol. 39, 7246-7253.

Phosphate capture by ultrathin MgAl layered double hydroxide nanoparticles

Chen Liu [a, c, g], Meiyi Zhang[*, a], Gang Pan[*, a, b, c], Laura Lundehøj [d], Ulla Gro Nielsen [d], Yi Shi [a, e] and Hans Christian Bruun Hansen [f, g]

[a] Research Center for Eco-Environmental Sciences, Chinese Academy of Sciences, Beijing 100085, China

[b] Center of Integrated Water-Energy-Food studies (iWEF), Nottingham Trent University, Nottinghamshire, NG25 0QF, UK

[c] University of Chinese Academy of Sciences, Beijing 100049, China

[d] Department of Physics, Chemistry and Pharmacy, University of Southern Denmark, Campusvej 55, 5230 Odense M, Denmark

[e] Shandong Key Laboratory of Water Pollution Control and Resource Reuse, School of Environmental Science and Engineering, Shandong University, Qingdao 266237, China

[f] Department of Plant and Environmental Sciences, University of Copenhagen, Thorvaldsensvej 40, DK-1871 Frederiksberg C, Denmark

[g] Sino-Danish Center for Education and Research (SDC), China

* Corresponding author: gpan@rcees.ac.cn (GP), myzhang@rcees.ac.cn

Abstract

Capture of phosphorus from runoff and wastewater is of high priority in order to reclaim phosphorus for food security and to prevent water pollution. Here we report an environmentally friendly method to synthesize ultrathin MgAl layered double hydroxide (LDH) nanoparticles for phosphorus adsorption. Fast co-precipitation of magnesium and aluminum at 25-80 °C in the presence of urea resulted in the desired LDH with variable admixtures of amorphous aluminum hydroxide (16-38%) quantified from solid state ^{27}Al MAS NMR. Freshly synthesized particles appeared as exfoliated single layers that upon drying stacked to form particles with thickness of 3 to 5 nm (four to six LDH layers) and lateral sizes of ~30 nm, as seen by XRD, SEM, TEM, and AFM. Phosphate adsorption on LDH nanoparticles synthesized at room temperature (LDHns-U25) was very fast and reaction reached equilibrium within 15 min at pH 8.5. The freeze-dried LDHns-U25 nanoparticles exhibited phosphate sorption capacity of 98±15 mg P g^{-1}, which is 55% higher than conventional LDH. Phosphate was bound to LDH electrostatically and via inner-sphere surface complexation as evidenced from a combination of ^{31}P MAS NMR spectroscopy, surface potential measurements, IR spectroscopy, and ionic strength effects on phosphate sorption. This study demonstrates that urea-facilitated synthesis of LDH nanoparticles provides fast and high capacity phosphate sorbents with potentials for phosphate recovery from waste waters.

Key words: Phosphate removal; Hydrotalcite-like compounds; Nanosheets; Adsorption; Wastewater

1. Introduction

Phosphorus is essential for agriculture and food security for the growing world population. However, excessive anthropogenic phosphate (P) arising from fertilization, treated municipal and industrial wastewater may cause eutrophication of receiving water bodies (Conley et al. 2009, Emmanuelawati et al. 2013, Shannon et al. 2008). Phosphorus capture and recycling is crucial, as phosphorus mineral deposits are being depleted (Pan et al. 2018, Reijnders 2014). Robust and efficient methods for P reduction at low cost and energy are therefore needed to address these challenges. Various technologies have been employed for phosphate removal from wastewaters, such as chemical precipitation, biological removal, ion exchange and adsorption. Among them, adsorption is promising due to less sludge production, high uptake capacity and efficiency at low P concentrations (Emmanuelawati et al. 2013, Moharami and Jalali 2013).

Layered double hydroxides (LDH) have been studied as sorbents for P removal due to their high anion-exchange capacity and their ability to accommodate different anions in the interlayer. LDH are layered structures comprising positively charged metal hydroxide layers typically comprising two different metal ions, interchanging with anionic interlayers of charge compensating anions（Das et al. 2003, Das et al. 2007, Mohapatra and Parida 2016). Here we refer to a specific LDH by the identity of the metal cations and the anion, e.g. MgAl-SO_4, for an LDH with magnesium and aluminum in the metal hydroxide layer and SO_4^{2-} in the interlayer. Promising P adsorption has been observed for MgAl-Cl, ZnAl-Cl, and ZnAl-NO_3 LDH from both synthetic solutions and waste waters (He et al. 2010, Kuzawa et al. 2006). New

generations of nanostructured adsorbents have been developed for P removal (Fang et al. 2015, Su et al. 2013) with high surface areas and abundant active adsorption sites. For instance, Zhang et al. (2015) reported a nano-$Mg(OH)_2$ modified polystyrene material exhibiting high adsorption capacity (45.6 mg P g^{-1}) for phosphate. However, the application of nanomaterials for wastewater cleaning has been challenged by complex manufacturing processes and use of toxic precursors.

Exfoliated LDH (here called LDH nanosheets) are interesting candidates as high capacity P adsorbents because they possess a permanent positive layer charge and a high specific surface area (Hibino and Jones 2001). A typical approach for formation of LDH nanosheets is to exfoliate pre-synthesized LDH layered compounds, usually by intercalation of large anionic solutes to weaken the interlayer interaction, followed by delamination of the modified products in organic solvents (Ma et al. 2006). However, the synthesis processes are time consuming and make use of costly (and toxic) organic solvents and reagents similar to other nano-adsorbents, which is a limitation for broader application.

In order to prevent stacking of the LDH nanosheets, one strategy is to introduce a stabilizer with high ability to form hydrogen bonds with hydroxyl groups as it may break the integrated bonding network among the hydroxyl groups of the metal hydroxide layers, the interlayer water molecules and anions (Wei et al. 2014). Formamide has been a classical agent for exfoliating LDH layers (Yu et al. 2015), but unfortunately makes synthesis unsustainable. Urea may represent a non-toxic alternative. The urea molecule has a high proportion of strongly electronegative

elements, one oxygen and two nitrogen atoms, implying a high capability of forming hydrogen bonds (Ma et al. 2006). Although homogeneous precipitation by thermal hydrolysis of urea - the so called ‘urea method’ (Costantino et al. 1998), results in LDH but with admixtures of amorphous Al-(hydr)oxide phases (Pushparaj et al. 2015), this method is frequently used for preparation of well-crystallized, large sized (2-20 μm) LDH under hydrothermal conditions (Adachi-Pagano et al. 2003, Hibino and Ohya 2009, Ogawa and Kaiho 2002). Progressive hydrolysis of urea usually produces hydroxide and carbonate ions, which are main components of the metal hydroxide layers and interlayers of LDH, and thus results in homogenous nucleation and crystallization of carbonate LDH (Hibino and Ohya 2009, Ogawa and Kaiho 2002) as well as formation of other layered phases (Staal et al. 2017). We hypothesize that a low reaction temperature may prevent urea hydrolysis, and thus that urea hydrates accumulate at the surface of LDH sheets, stabilizing the colloidal suspension, and causing the LDH layers to grow in-plane only and thus to produce LDH nanosheets.

In this study, we report a new route for directly synthesizing MgAl-NO_3 LDH nanosheet materials in urea solution. The P adsorption properties of this new material were studied with emphasis on adsorption kinetics, capacity and affinity as well as effects of solution pH and ionic strength. Solid state nuclear magnetic resonance (NMR) spectroscopy, zeta potential measurements, and Fourier transform infrared spectroscopy (FTIR) was used for characterization of the nanoparticles and P bonding.

2. Experimental

2.1 Materials

Magnesium nitrate ($Mg(NO_3)_2 \cdot 6H_2O$), aluminium nitrate ($Al(NO_3)_3 \cdot 9H_2O$), urea ($CO(NH_2)_2$), formamide (CH_3NO), concentrated nitric acid (HNO_3, 68 %), sodium hydroxide (NaOH, 98 %) and potassium dihydrogen phosphate (KH_2PO_4) were supplied by Sinopharm Chemical Reagent Co. (Beijing, China). All chemicals were of analytic grade (or higher), and was used without further purification. Deionized water was purged with high grade nitrogen (99.99%) for 30 min prior to use in order to remove carbon dioxide.

2.2 Synthesis of ultrathin LDH nanoparticles

Four different syntheses of MgAl-NO_3 LDH were performed in presence of urea at room temperature (LDHns-U25) and at 80°C (LDHns-U80), in formamide (LDHns-F), and by a conventional co-precipitation method (LDH-Ref), respectively. A 1 L solution containing $NaNO_3$ (0.01 M) and urea (6 M) was prepared in thermostatic water bath with pH adjusted to pH of 10.0 ± 0.5 using 0.5 M NaOH. A 200 mL mixed solution composed of 0.04 M $Al(NO_3)_3 \cdot 9H_2O$ and 0.08 M $Mg(NO_3)_2 \cdot 6H_2O$ was added dropwise (≈10-15 mL min^{-1}) to the beaker. Simultaneously, a solution of 0.5 M NaOH was added dropwise to maintain pH at 10.0 ± 0.5 under magnetic stirring (400 rpm) and N_2 flushing to avoid the entrance of CO_2 (30 mL min^{-1}) (Table 1). The pH was monitored using a Mettler Toledo combination pH electrode to ensure proper rate of NaOH addition. The resulting precipitate was collected by centrifugation for 15 min at 12840 g, washed twice with anhydrous ethanol and once with CO_2-free deionized water in sealed containers, and finally freeze-dried at -46°C for 24 h.

For comparison, LDHns-F was synthesized by modification of the method by Yu et al. (2015) using the same metal salt concentrations and the same reaction time as described above (Table 1). For reference, a conventional layered LDH-Ref was prepared using co-precipitation at constant pH similar to the method of Yun et al. (1995) (Table 1). The precipitate was stirred for 1 h and aged in water bath under stirring at 70°C for 24 h. All the other conditions were the same except formamide and urea was not added. The product was freeze-dried as described above.

Table 1. Composition of the solution, temperature and reaction time used for the synthesis of LDH.

2.3 Solid state characterization

The Mg and Al contents of the LDH samples were determined by inductively coupled plasma optical emission spectrometer (ICP-OES) and ^{27}Al magic angle spinning (MAS) NMR spectroscopy. The crystallinity, morphology and specific surface area of the LDHs synthesized were characterized by powder X-ray diffraction (XRD), field emission scanning electron microscopy (FESEM), transmission electronic microscopy (TEM), Atomic force microscopy (AFM), and Brunauer-Emmett-Teller N_2 adsorption (BET). A Zetasizer Nano ZS potential analyzer was used to measure the zeta potential of LDH particles in suspension before and after P adsorption. To study the phosphate speciation and bonding in the LDH, ^{31}P MAS NMR spectra and Transmission Fourier transform infrared spectroscopy (FTIR) were used. ^{27}Al MAS NMR spectroscopy was used to detect the presence of non-LDH impurities in the products, and to record LDH transformation when exposed to phosphate. Detailed

description of the measurements above can be found in the Supporting Information.

2.4 Phosphate adsorption

Phosphate adsorption kinetics was studied in batch experiments. Prior to use, the suspensions with a certain amount of freeze-dried LDH adsorbent dispersed in $NaNO_3$ electrolyte in polypropylene centrifuge tubes, were placed in an ultrasonic bath (80 kHz) for 30 min to minimize aggregation of LDH nanoparticles. Subsequently, various volumes of KH_2PO_4 solutions were added to the suspensions to yield a mixture volume of 30 mL, with LDH concentration of 1 g L^{-1} in 0.01 mol L^{-1} $NaNO_3$ background and different initial phosphate concentrations of 50 mg P L^{-1} and 80 mg P L^{-1}, respectively. The tubes were then shaken at 170 rpm for 8 h at 25±1°C, and the solution pH was kept constant at 8.5±0.1 using 0.1 M HNO_3/NaOH. The supernatant was separated by centrifugation after 3, 5, 7, 10, 15, 30, 60, 120, 240, 360, and 480 min at 12840 g for 5 min to determine the P concentration in the supernatants. The supernatants were filtered through a 0.22 μm polypropylene syringe filter and then analyzed for phosphate concentration using the molybdate colorimetric method at a wavelength of 880 nm using a spectrophotometer (UV-756 PC, Shanghai Sunny Hengping Scientific Instrument CO. LTD, China).

Adsorption isotherms were determined at pH 8.5±0.1 with the initial phosphate concentrations ranging from 10 to 120 mg P L^{-1} in presence of 1 g L^{-1} LDH and 0.01 M $NaNO_3$ electrolyte. The suspensions were constantly agitated for 24 h in a thermostatic shaker (25±1°C). After completion, suspensions were centrifuged, the supernatant sampled and the pellet re-dispersed in water to determine desorption of phosphate with

all experimental conditions maintained the same as during adsorption. Phosphate concentration was determined as described above. Adsorption data were fitted by the Langmuir isotherm model using non-linear regression in OriginPro 2016. The nitrate concentration of the solution after adsorption were measured by a colourimetric method (HACH, DR 1900).

In order to investigate how adsorption was affected by solution pH and ionic strength, 0.03 g freeze-dried LDH was added to 30 ml of 75 mg P L^{-1} solutions at three different electrolyte concentrations of 0.001, 0.01, or 0.1 M $NaNO_3$, respectively. The pH of the solution was adjusted from 7 to 11 using 0.1 M HNO_3/NaOH. After 24 h, the equilibrium pH was measured and the supernatants were filtered through 0.22 μm membrane for phosphate analysis.

3. Results and Discussion

3.1 Chemical and structural characterization of LDH nanoparticles

The phase composition of the synthesized freeze dried and gel-like fresh LDH was examined by powder-XRD (Fig. 1). When the freshly synthesized gel-like LDH product was examined, the basal reflections ((003) and (006)) were barely detectable (Fig. 1a), manifesting the lack of long-range order along the c-axis (Wang and O'Hare 2012, Yu et al. 2015). When samples were run as freeze-dried powder samples on a glass sample holder, a broad and intense basal reflection at 10.75° (0.82 nm) was observed demonstrating re-stacking of the colloidal LDH nanoparticles with nitrate in the interlayer (Fig. 1b) (Wu et al. 2005). The gel-like samples showed no signs of (003) basal reflections, but the characteristic (110) reflections was observed (Fig. 1a insert).

The cell parameter *a* (average metal-metal distance) calculated from the (110) reflection (X'Pert HighScore Plus) for dried LDHns-U25, LDHns-U80, LDHns-F and LDH-Ref samples were 3.054 Å, 3.048 Å, 3.048 Å and 3.045 Å, respectively. An *a* distance of 3.04 Å and 3.06 Å for Mg_2Al-NO_3 and Mg_3Al-NO_3 LDH, respectively have been observed by Hu1 and O'Hare (2005) and Wu et al. (2005), suggesting a Mg:Al ratio between 2:1 and 3:1 in our samples in agreement. Among the four samples, LDHns-U25 was synthesized at the lowest temperature, resulting in lowest intensity and broadest diffraction peaks (Fig. 1b). It can be concluded that direct synthesis in urea or formamide affords LDH nanoparticles with less crystallinity than that of traditional co-precipitation method.

Fig. 1. XRD patterns of (a) gel-like fresh sample of MgAl-LDH covered by Mylar film; inset: 110 reflection of gel-like fresh sample; (b) MgAl-LDH after freeze drying.

The purity of LDH preparations was further probed by ^{27}Al MAS NMR spectroscopy (Fig. 2). The asymmetric line shape of the isotropic resonance is characteristic for MgAl-LDH with impurities of amorphous aluminum hydroxides (AOH), see Pushparaj et al. (2015) and Staal et al. (2017) for a detailed discussion. Deconvolution of the ^{27}Al MAS NMR spectra allowed for an estimate of the relative concentration of the AOH phase admixture in the samples ranging between 16 and 38% (Fig. 2, Table S2). The admixture of AOH phases was expected given the fast metal salt addition, very short aging and absence of post synthesis treatment (Pushparaj et al. 2015). The relative AOH content was lower (16%) for the samples synthesized at 80°C

than for the samples prepared at 25°C (38%); hence the formation of AOH is temperature dependent, as observed earlier for co-precipitation (Pushparaj et al. 2015). In addition, all the samples contain less than 5% of tetrahedrally coordinated Al as seen from shifts at approx. 64 and 74 ppm, which most likely originates from a colloidal aluminum hydroxide gel (Staal et al. 2017).

The physiochemical properties of the LDH-Ref and the three LDH nanoparticle samples are summarized in Table 2. The bulk Mg:Al ratios of LDHns-F, LDHns-U25, LDHns-U80, and LDH-Ref samples were 1.97, 1.90, 2.10, and 1.91, respectively (calculated from ICP-OES), which are close to the Mg:Al ratios in the synthesis mixture. However, the actual Mg:Al ratios in LDH is higher (Table 2) because only 75±5 to 84±5 % of the total Al is in the LDH phase based on ^{27}Al SSNMR (Table S2), i.e., the LDH is depleted in Al as compared to the bulk composition (Staal et al. 2017) (see above). The N_2-adsorption/desorption isotherms of the LDH samples were analyzed to determine their specific surface areas and porosity (Fig. S2). The hysteresis loops display no limiting adsorption at high P/P_0, which is common for plate-like particles with slit-shaped pores (Zhan et al. 2016). All specific surface areas of the LDH nanoparticles (83-97 m^2 g^{-1}) were higher than that of LDH-Ref (52 m^2 g^{-1}, Table 2). The LDH samples display a distinct H3-type hysteresis loop (P/P_0 > 0.4), implying the presence of mesopores (2-50 nm). The average pore diameters of all the samples are small with a narrow distribution below 20 nm, indicating a mesoporous structure.

Fig. 2. Deconvolutions of the ^{27}Al MAS NMR spectra of the MgAl-LDH nanoparticles,

a) LDHns-F, b) LDHns-U80, c) LDHns-U25, d) LDHns-F_P, e) LDHns-U80_P and f) LDHns-U25_P. The experimental spectrum (Exp), simulated (Sim) and difference (Dif) are shown for each. The results are summarized in Table S2.

Table 2. Composition, BET and pore sizes of pristine LDH and nanoparticle samples

TEM images (Fig. 3) show that the three LDH samples synthesized in presence of formamide or urea have a sheet-like structure with a lateral size of ~30 nm, and a thickness of ~5 nm, respectively. The urea synthesis products are a few nanometers thick, evidenced by the slender dark colored area (Fig. 3a-b), where some of the particles are obviously curled. Sample LDHns-U25 (Fig. 3a) consists of very small, less well defined and highly aggregated particles which probably is due to a relatively high amount of AOH in this sample compared to its counterparts that were synthesized at 80°C (Table S2). The inset in Fig. 3c displays the basal plane of an individual LDH hexagon. The representative SEM images of the samples (Figure S3, Supporting Information) also confirm the formation of ultrathin sheet-like morphology.

Fig. 3. TEM images of LDH nanoparticles: a): LDHns-U25; b): LDHns-U80; c): LDHns-F; (d) AFM image and the corresponding height profile for the marked line in the image for LDHns-U25 mapped in ScanAsyst mode, height image over scanning area of 200×200 nm^2.

To further quantify the thickness of LDH nanoparticles, the freeze-dried materials were examined by AFM. The height profile along transects across particles are shown

in Fig. 3d, which reveals a particle thickness of 3 to 5 nm. Fig. 3d displays sheet-like objects with a similar lateral size as observed by TEM (Fig. 3c). The thickness for a single metal hydroxide layer with the interlayer is 0.8 nm as seen from XRD (Fig.1b). Particles with thicknesses of 3 to 5 nm thus consist of approximately four to six layers (Li et al. 2005, Ma et al. 2006). These compelling evidences confirm the formation of LDH nanoparticles with a thickness of only few layers consistent with previous studies of exfoliated layered LDH (Fang et al. 2015, Hibino and Jones 2001, Ma et al. 2006). For comparison, the AFM image of LDH-Ref along with the corresponding height profile is shown in Fig. S4. The size of LDH-Ref is larger compared to LDH nanoparticles, with diameter of 100-150 nm and thickness of higher than 14 nm. This may due to long crystallization time of the synthesis process.

3.2 Phosphate adsorption

The kinetics of phosphate adsorption to LDHns-U25 at different initial phosphate concentrations were well fitted by a pseudo second-order model (eqn. (1)) (Fig. 4a, parameters in Table S3).

$$\frac{t}{q_t} = \frac{1}{k_2 q_e^2} + \frac{1}{q_e} t \qquad (1)$$

where q_t is the adsorbed amount at a time t (mg g^{-1}), q_e is the adsorbed amount at equilibrium, and k_2 (g mg^{-1} min^{-1}) the rate constant. Phosphate adsorption occurred rapidly and reached equilibrium within 15 min. Similar fast adsorption (within 15 min) has been observed by ultrathin γ-Fe_2O_3 nanosheets (Liu et al. 2016). Phosphate adsorption to LDHns-U25 is fast, compared to many other layered MgAl-LDH, which the equilibrium time will take from 40 min to a few hours (Das et al. 2006, Yang et al.

2014, Khitous, M. et al. 2015). For metal oxides, the equilibrium time will be several hours (Ren et al. 2012, Yu and Chen 2015).

Fig. 4. a) Kinetics of phosphate adsorption to LDHns-U25 and corresponding pseudo-second-order kinetics (eqn(1)); b) Adsorption isotherms for phosphate adsorption to pristine LDH and LDH nanoparticles and the corresponding Langmuir fits (error bars represent the standard deviation of duplicates).

Table 3. Langmuir isotherm parameters of the LDH.

Isotherm data were well described by the Langmuir model (eqn(2)) (Fig. 4b, Table 3).

$$q_{\mathrm{e}} = \frac{K_{\mathrm{L}} C_{\mathrm{e}} q_{\mathrm{m}}}{1 + K_{\mathrm{L}} C_{\mathrm{e}}} \qquad (2)$$

where C_{e} (mg P L^{-1}) is the equilibrium phosphate concentration in solution, q_{e} (mg P g^{-1}) the amount of phosphate adsorbed, q_{m} (mg P g^{-1}) the maximum adsorption capacity, and K_{L} (L mg$(P)^{-1}$) the Langmuir affinity constant. The maximum phosphate adsorption capacity obtained from Langmuir fitting follows this sequence: LDHns-U25 > LDHns-F > LDHns-U80 > LDH-Ref, with q_{m} spanning from 98.3±14.6 mg P g^{-1} to 63.5±8.6 mg P g^{-1}. Desorption of phosphate from the phosphate loaded nanoparticles was evaluated after adsorption experiments by replacement of the solution with fresh electrolyte without phosphate, and controlling pH at 8.5. The extent of phosphate desorption was calculated by dividing the desorbed amount after 24 h by the initial adsorbed amount. Phosphate desorption from LDHns-U25 and LDHns-U80 were low, with the lowest values of 0.17±0.03% and 0.82±0.04% at low P loadings, and

the highest of 5.04±0.28% and 6.23±0.21% at high P loadings (Fig. 5a). Thus, desorption from LDH nanoparticles is low, hence increasing the potential of the LDH materials for water cleaning.

Fig. 5b reveals the effects of pH and ionic strength on phosphate adsorption by LDHns-U25. In the studied pH range 7-11, phosphate adsorption dropped significantly from ~73 to ~42 mg g^{-1} with increasing pH. Similar solution pH effect on phosphate adsorption has also been observed for Mg-Al LDH (Yang et al. 2014). The protonation of the hydroxyl groups of the MgAl hydroxide layers will change with pH contributing with positive surface charge at low pH and negative surface charge at high pH. At higher pH, LDH layers become increasingly deprotonated and causes electrostatic repulsion between phosphate and deprotonated surface OH groups (Chitrakar et al. 2006). Thus, the change in charge of phosphate ion, the change in charge of the LDH metal hydroxide layers and competition with OH^- jointly cause adsorption to decrease with increasing pH. Furthermore, competition with carbonate is also more prevalent at high pH due to the unfavorable shift in the CO_2-equilibrium (Lundehøj et al, 2019).

Increasing the ionic strength from 0.001 M to 0.1 M had no significant effect on adsorption (Fig. 5b). This is a strong indication that adsorption may take place via inner-sphere surface complexation (McBride 1997, Su et al. 2013, Zhang et al. 2009) which is insensitive to ionic strength as opposed to outer-sphere surface complexation that decreases with increasing ionic strength (Su et al. 2013). Thus, the results suggest that phosphate form inner-sphere complexes when adsorbed on LDH nanoparticles.

Fig. 5. (a) Phosphate desorption from LDH nanoparticles (pH 8.5±0.1, desorption time: 24 h); (b) The effect of pH and ionic strength on phosphate adsorption by LDHns-U25 (error bars represent the standard deviation of duplicates).

3.3 Phosphate bonding to LDH nanoparticles

3.3.1 Solid state NMR

^{27}Al MAS NMR spectra of LDH nanoparticles were recorded after exposure to phosphate. The deconvolutions of these spectra showed no significant changes in the relative concentration for the LDH component, indicating that the LDH is not dissolved or transformed when exposed to phosphate. ^{27}Al MAS NMR spectra of the LDH nanoparticles after phosphate adsorption showed a small (0.5-0.7 ppm) change in δ_{iso} (^{27}Al) indicating incorporation of phosphate in the interlayer of the LDH. ^{31}P MAS NMR spectra were used to study phosphate speciation and bonding in the LDH. The ^{31}P MAS NMR spectra contain one resonance, accompanied by a few weak spinning side bands (Table 4, Fig. 6). These results are in good agreement with earlier studies on MgAl-LDH (Hou et al. 2003). The presence of multiple ^{31}P sites imply that in addition to electrostatic bonding in their interlayer, phosphate may also form surface complexes on e.g., the edges and outside of the particles. In addition, phosphate also sorb to AOH present in the LDH nanoparticle samples according to ^{27}Al SSNMR (Table S2); We assign the broad resonance at δ_{iso}(^{31}P) ≈ -9 ppm to phosphate adsorbed to AOH and possibly a small amount of an amorphous aluminum phosphate ($AlPO_4$) phase based on our recent study of phosphate adsorption on ZnAl-LDH in acidified waste water sludge (Lundehøj et al 2019). We note that the

^{27}Al SSNMR spectra of the P-loaded samples have a small intensity (< 5 %) in the region 0 to -5 ppm for $AlPO_4$, but could not be determined precisely from deconvolution. This P-AOH resonance constitute 6(4) to 12(6) % of the total P c.f., Figure 6. Thus, phosphate sorbed to the AOH component is less than 15% of the sorption maximum.

Table 4. Parameters obtained from the deconvolutions of the ^{31}P MAS NMR spectra

Fig. 6. Deconvolution of the experimental ^{31}P MAS NMR spectra of the MgAl-LDH nanosheets exposed to phosphate. a) LDHns-F_P, b) LDHns-U80_P, and c) LDHns-U25_P. The experimental spectrum (Exp), simulated (Sim) and difference (Dif) are shown for each.

3.3.2 Surface zeta potentials

Fig. 7a shows the zeta potentials of pure LDH nanoparticles before and after exposure to 50 mg P L^{-1} phosphate solution. Before the adsorption, the surface charge of LDH nanoparticles is positive in the studied pH range, but a decline is seen with increasing pH as the surface OH groups are increasingly deprotonated (Hansen and Koch 1995). After phosphate adsorption, the surface charge of LDH nanoparticles decreased significantly, and the isoelectric point of LDHns-U25 and LDHns-U80 was determined to pH 5.3 and 5.7, respectively. The marked decrease of the zeta potential after phosphate adsorption indicates that phosphate adsorbed to LDH nanosheet surfaces is bound as inner-sphere surface complexes as formation of outer-sphere surface complexes cannot shift the surface charge of this magnitude (Ren et al. 2012, Su

et al. 2013, Yang et al. 2014).

Fig. 7. a) Zeta potential of LDHns-U25 and LDHns-U80 before (solid line) and after (dot line) phosphate adsorption with initial phosphate concentration of 50 mg L^{-1}, adsorbent dose at 1g L^{-1}; b) FT-IR spectra of LDHns-U25 before (A) and after (B_{1-4}) phosphate adsorption at different phosphate initial concentrations: B_1= 20 mg L^{-1}, B_2= 50 mg L^{-1}, B_3= 80 mg L^{-1}, B_4= 120 mg L^{-1}.

3.3.3 FT-IR analysis

The FT-IR spectrum of non-treated LDHns-U25 is compared with the P-loaded sorbents at several different initial P concentrations (Fig. 7b). The strong and broad bands at 3453 cm^{-1} and 1632 cm^{-1} belong to the stretching and bending vibration of the hydroxyl groups (–OH) in the LDH metal hydroxide layers and water, respectively (Liu et al. 2010, Zhang et al. 2005). The bands at ca.1384 cm^{-1} are identified as υ_3 mode of NO_3^- (Wu et al. 2005) in the interlayer. The hydrolysis of urea proceeds in two steps, with first formation of NH_4CNO (2200 cm^{-1}) and next formation of ammonium and carbonate (Adachi-Pagano et al. 2003). However, none of these bands were observed in the IR spectra demonstrating that urea was not decomposed during synthesis (Benito et al. 2008). After reaction with phosphate solution, a new, broad band at 1059-1067 cm^{-1} appeared, which can be assigned to the symmetrical stretching vibration of phosphate (Yu and Chen 2015). Its intensity increased with the phosphate concentration used indicating that the surface hydroxyl groups were replaced by the adsorbed phosphate via formation of an inner-sphere surface complex (M-O-P) between phosphate and the

LDH metal hydroxide layers (Lǔ et al. 2013, Yu and Chen 2015, Zhan et al. 2016), in accordance with the results of ionic strength and zeta potential measurements. The 1384 cm^{-1} peak (NO_3^-) decreased with increasing phosphate concentration, in accordance with decreasing nitrate concentration from 10 to 3.4 mmol l^{-1} after adsorption, suggesting that competitive adsorption exists between phosphate anions and nitrate in the solution. This could be attributed to much higher concentration of $NaNO_3$ electrolyte than phosphate in the solution.

A simple calculation accounting for the charge of the LDH interlayer and the charge of the phosphate anion provides an estimate of the maximum amount of phosphate (HPO_4^{2-}) that can be adsorbed due to electrostatic bonding (Supporting Information). The estimated amounts represent 50-70% of the maximum P adsorption capacity. Thus, other modes of adsorption than electrostatic bonding are active. The observation of four different environments in the ^{31}P NMR spectra support the adsorption on the surface of the particles and intercalation of P in the interlayer. The latter was also confirmed by a slight increase of d-spacing after P adsorption (Fig. S1, Table S1) (Hansen 1995). The little change in interlayer spacing after intercalation is in agreement with the findings in Gillman et al. (2008). This could be attributed to non-uniform distribution of phosphate/water in the interlayers (Gillman et al. 2008). The adsorption mechanism on LDH can be speculated as illustrated in Fig.8: there was electrostatic attraction between negatively charged phosphate species and positively charged LDH nanoparticles; inner-sphere surface complexation may be formed when phosphate was adsorbed on the surface of the LDH nanoparticles; ion exchange

between phosphate anions and interlayer NO_3^-.

Fig. 8. The possible synthesis process and P adsorption mechanisms by LDH nanoparticles（Yang et al. 2014）.

3.4 Perspectives for applications

Table S4 compares the maximum adsorption capacities of various adsorbents for phosphate. It is found that the LDH nanoparticles produced in this work have a significantly higher phosphate removal capacity than many other adsorbents, e.g. granular MgAl LDH (hydrotalcite) (Kuzawa et al. 2006), hydrotalcite (Ookubo at al. 1993), MgAl LDH (Yang et al. 2014), gibbsite (Lookman et al. 1997), goethite (Kim et al. 2011), and phoslock, a commercial lanthanum exchanged bentonite which is used for trapping P in lake restauration (Robb et al. 2003, Ross et al. 2008, Spears et al. 2013, Xu et al. 2017). A high adsorption capacity of our LDH nanoparticles compared to other layered LDH may be attributed to the thin particles contributing a high density of adsorption sites that are not accessible in thicker LDH particles (Fang et al. 2015). The remarkably high adsorption capacity of 131 mg P g^{-1} for CaAl LDH (hydrocalumite) is due to precipitation of calcium phosphates as the LDH dissolves (Xu et al. 2010). Amorphous aluminum hydroxide which is present in our samples (Fig. S4) has an adsorption capacity less than half of that for LDHns-U25. Many adsorbents including iron oxides (Lǔ et al. 2013, Zhang et al. 2009) and zirconium oxides (Su et al. 2013) often have negative surface charges at the pH of natural waters and thus sorption may be rather low even at pH 7 (Xu et al. 2017). On the contrary, LDH nanoparticles

can be used even at high pH which may be encountered during eutrophication events such as cyanobacterial blooms (pH～8.5).

4. Conclusion

This study presents a facile method for the synthesis of Mg-Al LDH nanoparticles using urea as a dispersing agent to limit layer stacking. The mesoporous material consists of platy particles with a thickness of 3-5 nm and diameters of approximately 30 nm contributing to a specific surface area of 84 m^2 g^{-1}. The freshly synthesized and non-aged products contain variable amounts of admixed AOH (16-38%). The LDH nanoparticles show very fast (15 min) phosphate adsorption and a high phosphate adsorption capacity of close to 100 mg P g^{-1} at pH 8.5. The ^{31}P MAS NMR spectroscopy showed that phosphate adsorption occurs by intercalation in the interlayer (ion exchange) and inner-sphere surface complexation. The latter was confirmed by ionic strength effects on adsorption, zeta-potential measurements and IR spectroscopy. NMR showed the LDH to be stable during phosphate adsorption and less than 7% of adsorbed P desorbed on 24 h desorption tests. Easy, cheap and environmentally friendly synthesis, fast and high capacity adsorption even for high pH waters and low phosphate desorption makes the new LDH adsorbent interesting for treatment of waste waters or phosphate rich runoff.

Acknowledgements

This work was financially supported by National Key R&D Program of China [grant numbers 2017YFA0207204], and National Natural Science Foundation of China [grant numbers 21377003], the Villum Foundation via the “Villum Young Investigator

Programme" [grant numbers VKR022364] (UGN, LL), the Innovation Foundation, Denmark (ReCoverP), Sino-Danish Center and Beijing Natural Science Foundation [grant numbers 8162040].

References

Adachi-Pagano, M., Forano, C., Besse, J.-P., 2003. Synthesis of Al-rich hydrotalcite-like compounds by using the urea hydrolysis reaction-control of size and morphology. J. Mater. Chem. 13, 1988-1993.

Benito, P., Herrero, M., Barriga, C., Labajos, F.M., Rives, V., 2008. Microwave-assisted homogeneous precipitation of hydrotalcites by urea hydrolysis. Inorg. Chem. 47, 5453-5463.

Chitrakar, R., Tezuka, S., Sonoda, A., Sakane, K., Ooi, K., Hirotsu, T., 2006. Selective adsorption of phosphate from seawater and wastewater by amorphous zirconium hydroxide. J. Colloid Interface Sci. 297, 426-433.

Conley, D.J., Paerl, H.W., Howarth, R.W., Boesch, D.F., Seitzinger, S.P., Havens, K.E., Lancelot, C., Likens, G.E., 2009. Controlling eutrophication: nitrogen and phosphorus. Science 323, 1014-1015.

Costantino, U., Marmottini, F., Nocchetti, M., Vivani, R., 1998. New synthetic routes to hydrotalcite-like compounds-characterisation and properties of the obtained materials. Berichte Der Deutschen Chemischen Gesellschaft, 1439-1446.

Das, D.P., Das, J. and Parida, K.,2003. Physicochemical characterization and adsorption behavior of calcined Zn/Al hydrotalcite-like compound (HTlc) towards removal of fluoride from aqueous solution. J. Colloid Interface Sci.

261(2), 213-220.

Das, J., Patra, B.S., Baliarsingh, N., Parida, K.M., 2006. Adsorption of phosphate by layered double hydroxides in aqueous solutions. Appl. Clay Sci. 32, 252-260.

Das, J., Patra, B.S., Baliarsingh, N., Parida, K.M., 2007. Calcined Mg-Fe-CO_3 layer double hydroxide as an adsorbent for the removal of selenite. J. Colloid Interface Sci. 316, 216-223.

Emmanuelawati, I., Yang, J., Zhang, J., Zhang, H.W., Zhou, L., Yu, C.Z., 2013. Low-cost and large-scale synthesis of functional porous materials for phosphate removal with high performance. Nanoscale 5, 6173-6180.

Fang, L., Huang, L., Holm, P.E., Yang, X., Hansen, H.C.B., Wang, D., 2015. Facile upscaled synthesis of layered iron oxide nanosheets and their application in phosphate removal. J. Mater. Chem. A 3, 7505-7512.

Gillman, G., Noble, M. and Raven, M.D.,2008. Anion substitution of nitrate-saturated layered double hydroxide of Mg and Al. Applied Clay Science 38(3-4), 179-186.

Hansen, H.C.B., 1995. Interlayer bonding of orthophosphate and orthosilicate in layered magnesium-aluminium hydroxide (hydrotalcite), International Clay Conference, pp. 201-206.

Hansen, H.C.B., Koch, C.B., 1995. Synthesis and characterization of pyroaurite. Appl. Clay Sci. 10, 5-19.

He, H., Kang, H., Ma, S., Bai, Y., Yang, X., 2010. High adsorption selectivity of ZnAl layered double hydroxides and the calcined materials toward phosphate. J. Colloid Interface Sci. 343, 225-231.

Hibino, T., Jones, W., 2001. New approach to the delamination of layered double hydroxides. J. Mater. Chem. 11, 1321-1323.

Hibino, T., Ohya, H., 2009. Synthesis of crystalline layered double hydroxides: Precipitation by using urea hydrolysis and subsequent hydrothermal reactions in aqueous solutions. Appl. Clay Sci. 45, 123-132.

Hou, X., Bish, D.L., Wang, S.L., Johnston, C.T., Kirkpatrick, R.J., 2003. Hydration, expansion, structure, and dynamics of layered double hydroxides. Am. Mineral. 88, 167-179.

Hu, G., O'Hare, D., 2005. Unique layered double hydroxide morphologies using reverse microemulsion synthesis. J. Am. Chem. Soc., 17808-17813.

Khitous, M., Salem, Z. and Halliche, D.,2015. Removal of phosphate from industrial wastewater using uncalcined MgAl-NO_3 layered double hydroxide: batch study and modeling. Desalination & Water Treatment 57, 1-12.

Kim, J., Li, W., Philips, B.L., Grey, C.P., 2011. Phosphate adsorption on the iron oxyhydroxides goethite (α-FeOOH), akaganeite (β-FeOOH), and lepidocrocite (γ-FeOOH): a ^{31}P NMR Study. Energy Environ. Sci. 4, 4298-4305.

Kuzawa, K., Jung, Y.J., Kiso, Y., Yamada, T., Nagai, M., Lee, T.G., 2006. Phosphate removal and recovery with a synthetic hydrotalcite as an adsorbent. Chemosphere 62, 45-52.

Li, L., Ma, R., Ebina, Y., Nobuo Iyi, A., Sasaki, T., 2005. Positively charged nanosheets derived via total delamination of layered double hydroxides. Chem. Mater. 17, 4386-4391.

Liu, H., Deng, S., Li, Z., Yu, G., Huang, J., 2010. Preparation of Al–Ce hybrid adsorbent and its application for defluoridation of drinking water. J. Hazard. Mater. 179, 424-430.

Liu, R., Liu, J.F., Zhang, L., Sun, J. and Jiang, G.,2016. Low temperature synthesized ultrathin γ-Fe_2O_3 nanosheets show similar adsorption behavior for As(III) and As(V). J. Mater. Chem. A 4, 7606-7614.

Lookman, R., Grobet, P., Merckx, R., Van Riemsdijk, W.H., 1997. Application of ^{31}P and ^{27}Al MAS NMR for phosphate speciation studies in soil and aluminium hydroxides: promises and constraints. Geoderma 80, 369-388.

Lǔ, J., Liu, H., Liu, R., Zhao, X., Sun, L., Qu, J., 2013. Adsorptive removal of phosphate by a nanostructured Fe–Al–Mn trimetal oxide adsorbent. Powder Technol. 233, 146-154.

L. Lundehøj H.C. Jensen, L. Wybrandt, U. G. Nielsen, M.L. Christensen, C. A. Quist-Jensen., 2019. Layered double hydroxides for phosphorus recovery from acidified and non-acidified dewatered sludge. Water Res. https://doi.org/10.1016/j.watres. 2019.01.004

Ma, R.Z., Liu, Z.P., Li, L., Iyi, N., Sasaki, T., 2006. Exfoliating layered double hydroxides in formamide: a method to obtain positively charged nanosheets. J. Mater. Chem. 16, 3809-3813.

McBride, M.B., 1997. A critique of diffuse double layer models applied to colloid and surface chemistry. Clays Clay Miner. 45, 598-608.

Mohapatra, L. and Parida, K.,2016. A review on recent progress, challenges and perspective of layered double hydroxides as promising photocatalysts. J. Mater.

Chem. A 4, 10744-10766.

Moharami, S., Jalali, M., 2013. Removal of phosphorus from aqueous solution by Iranian natural adsorbents. Chem. Eng. J. 223, 328-339.

Ogawa, M., Kaiho, H., 2002. Homogeneous precipitation of uniform hydrotalcite particles. Langmuir 18, 4240-4242.

Ookubo, A., Ooi, K. and Hayashi, H.,1993. Preparation and phosphate ion-exchange properties of a hydrotalcite-like compound. Langmuir 9, 1418-1422.

Pan, G., Lyu, T., Mortimer, R.J., 2018. Closing phosphorus cycle from natural waters: re-capturing phosphorus through an integrated water-energy-food strategy. J. Environ. Sci. 65, 375-376.

Pushparaj, S.S.C., Forano, C., Prevot, V., Lipton, A.S., Rees, G.J., Hanna, J.V., Nielsen, U.G., 2015. How the method of synthesis governs the local and global structure of zinc aluminum layered double hydroxides. J. Phys. Chem. C 119, 27695-27707.

Reijnders, L., 2014. Phosphorus resources, their depletion and conservation, a review. Resour. Conserv. Recycl. 93, 32-49.

Ren, Z., Shao, L., Zhang, G., 2012. Adsorption of phosphate from aqueous solution using an Iron–Zirconium binary oxide sorbent. Water, Air, Soil Pollut. 223, 4221-4231.

Robb, M., Greenop, B., Goss, Z., Douglas, G., Adeney, J., 2003. Application of Phoslock (TM), an innovative phosphorus binding clay, to two Western Australian waterways: preliminary findings. Hydrobiologia 494, 237-243.

Ross, G., Haghseresht, F., Cloete, T.E., 2008. The effect of pH and anoxia on the performance of Phoslock® , a phosphorus binding clay. Harmful Algae 7, 545-550.

Shannon, M.A., Bohn, P.W., Elimelech, M., Georgiadis, J.G., Marinas, B.J., Mayes, A.M., 2008. Science and technology for water purification in the coming decades. Nature 452, 301-310.

Spears, B.M., Lurling, M., Yasseri, S., Castro-Castellon, A.T., Gibbs, M., Meis, S., McDonald, C., McIntosh, J., Sleep, D., Van Oosterhout, F., 2013. Lake responses following lanthanum-modified bentonite clay (Phoslock) application: an analysis of water column lanthanum data from 16 case study lakes. Water Res. 47, 5930-5942.

Staal, L.B., Pushparaj, S.S.C., Forano, C., Prevot, V., Ravnsbaek, D.B., Bjerring, M., Nielsen, U.G., 2017. Competitive reactions during synthesis of zinc aluminum layered double hydroxides by thermal hydrolysis of urea. J. Mater. Chem. A 5, 21795-21806.

Su, Y., Cui, H., Li, Q., Gao, S., Shang, J.K., 2013. Strong adsorption of phosphate by amorphous zirconium oxide nanoparticles. Water Res. 47, 5018-5026.

Wang, Q., O'Hare, D., 2012. Recent advances in the synthesis and application of layered double hydroxide (LDH) nanosheets. Chem. Rev. 112, 4124-4155.

Wei, Y., Li, F., Liu, L., 2014. Liquid exfoliation of Zn–Al layered double hydroxide using NaOH/urea aqueous solution at low temperature. Rsc Adv. 4, 18044-18051.

Wu, Q., Olafsen, A., Vistad, Ø.B., Roots, J., Norby, P., 2005. Delamination and restacking of a layered double hydroxide with nitrate as counter anion. J. Mater. Chem. 15, 4695-4700.

Xu, R., Zhang, M., Mortimer, R.J., Pan, G., 2017. Enhanced Phosphorus Locking by Novel Lanthanum/Aluminum-Hydroxide Composite: Implications for Eutrophication Control. Environ. Sci. Technol. 51, 3418-3425.

Xu, Y., Dai, Y., Zhou, J., Xu, Z.P., Qian, G., Lu, G.Q.M., 2010. Removal efficiency of arsenate and phosphate from aqueous solution using layered double hydroxide materials: intercalation vs. precipitation. J. Mater. Chem. 20, 4684-4691.

Yang, K., Yan, L.G., Yang, Y.M., Yu, S.J., Shan, R.R., Yu, H.Q., Zhu, B.C., Du, B., 2014. Adsorptive removal of phosphate by Mg–Al and Zn–Al layered double hydroxides: Kinetics, isotherms and mechanisms. Sep. Purif. Technol. 124, 36-42.

Yu, J., Martin, B.R., Clearfield, A., Luo, Z., Sun, L., 2015. One-step direct synthesis of layered double hydroxide single-layer nanosheets. Nanoscale 7, 9448-9451.

Yu, Y., Chen, J.P., 2015. Key factors for optimum performance in phosphate removal from contaminated water by a Fe-Mg-La tri-metal composite sorbent. J. Colloid Interface Sci. 445, 303-311.

Zhan, T., Zhang, Y., Yang, Q., Deng, H., Xu, J., Hou, W., 2016. Ultrathin layered double hydroxide nanosheets prepared from a water-in-ionic liquid surfactant-free microemulsion for phosphate removal from aquatic systems. Chem. Eng. J. 302, 459-465.

Zhang, G., Liu, H., Liu, R., Qu, J., 2009. Removal of phosphate from water by a Fe-Mn binary oxide adsorbent. J. Colloid Interface Sci. 335, 168-174.

Zhang, Q., Zhang, Z., Teng, J., Huang, H., Peng, Q., Jiao, T., Hou, L., Li, B., 2015. Highly efficient phosphate sequestration in aqueous solutions using nanomagnesium hydroxide modified polystyrene materials. Ind. Eng. Chem. Res. 54, 2940–2949.

Zhang, Y., Yang, M., Dou, X, He, H., Wang, D., 2005. Arsenate adsorption on an Fe−Ce bimetal oxide adsorbent: role of surface properties. Environ. Sci. Technol. 39, 7246-7253.

Graphical Abstract

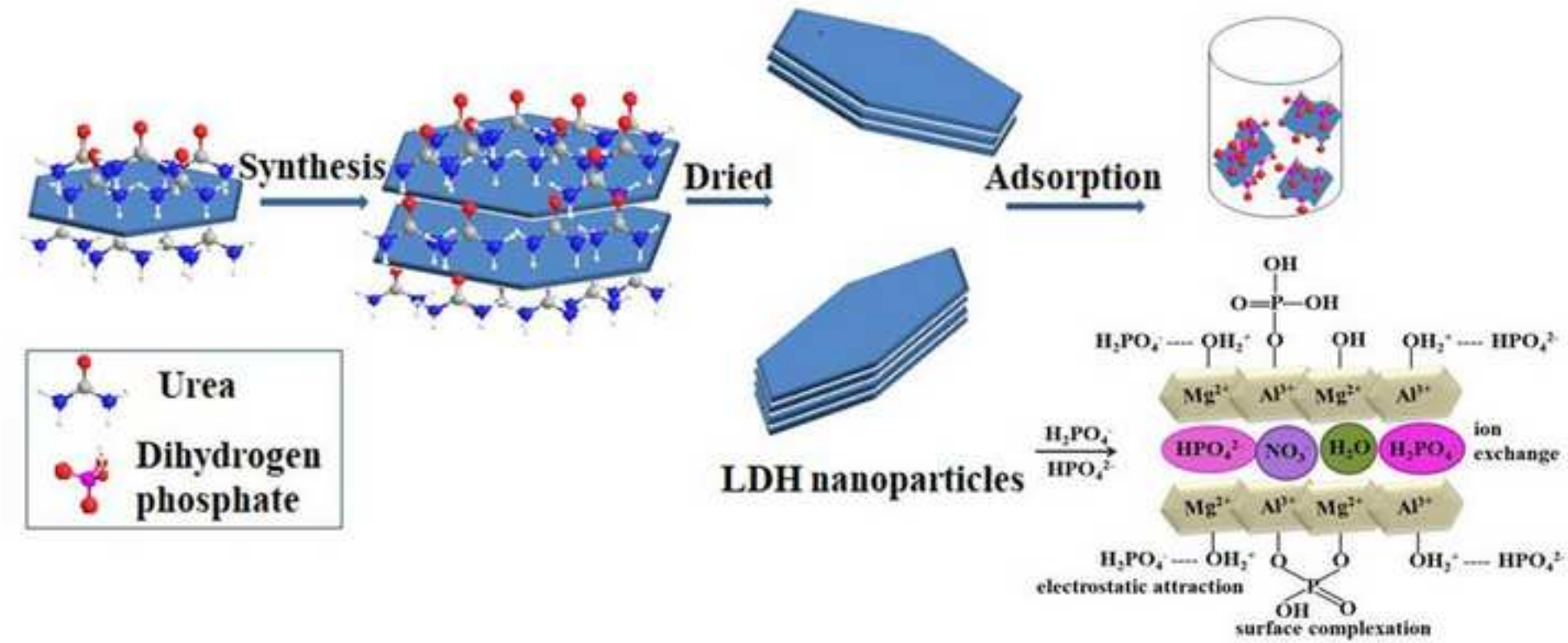

Highlights:

- Fast one-step LDH synthesis of 3-5 nm thick nanoparticles using urea as a dispersing agent
- The freeze-dried LDH nanoparticles exhibits high phosphate adsorption capacity (98 mg P g^{-1}) and fast sorption kinetics (15 min)
- Phosphate binds to LDH by inner-sphere surface complexation and by intercalation

Table 1. Composition of the solution, temperature and reaction time used for the synthesis of LDH.

Sample	Formamide (M)	Urea (M)	Temperature (°C)	Time (min)
LDHns-F	5.8	0.0	80	15
LDHns-U80	0.0	5.8	80	15
LDHns-U25	0.0	5.8	25	15
LDH-Ref	0.0	0.0	70	1440

Table
Click here to download Table: Table 2.docx

Table 2. Composition, BET and pore sizes of pristine LDH and nanoparticle samples

Sample	Surface area (m^2 g^{-1})	Pore volume (cm^3 g^{-1})	Average pore diam (nm)	Mg content (mmol g^{-1})	Al content (mmol g^{-1})	Actual Mg:Al atomic ratio[a]
LDH-Ref	52.0	0.11	7.2	8.33±0.13	4.37±0.04	-[b]
LDHns-F	83.3	0.25	16.1	8.67±0.28	4.41±0.20	2.63±0.02
LDHns-U25	84.0	0.26	19.0	9.00±0.43	4.74±0.28	3.06±0.02
LDHns-U80	97.0	0.28	13.0	9.00±0.35	4.30±0.15	2.50±0.01

[a] The values were determined by chemical analysis and amount of AOH from ^{27}Al SSNMR; [b] not measured

Table 3. Langmuir isotherm parameters of the LDH.

Adsorbent	q_m (mg g^{-1})	K_L (L mg^{-1})	R^2
LDH-Ref	63.5±8.6	0.099±0.035	0.931
LDHns-F	89.6±11.1	0.145±0.058	0.913
LDHns-U25	98.3±14.6	0.141±0.064	0.900
LDHns-U80	97.6±11.2	0.072±0.021	0.956

Table 4. Parameters obtained from the deconvolutions of the ^{31}P MAS NMR spectra

Sample	$\delta_{iso}(^{31}P)$ (ppm)	I [%]
LDHns-F80-P	-8.3(8)	12(6)
	-1.5(6)	43(7)
	3.4(4)	38(7)
	8.7(4)	7(4)
LDHns-U80-P	-9.2(8)	7(4)
	-2.0(6)	37(7)
	3.3(4)	49(7)
	9.1(4)	7(4)
LDHns-U25-P	-9.4(8)	6(4)
	-3.1(6)	34(7)
	2.4(4)	57(7)
	8.9(4)	3(2)

Figure
Click here to download Figure: Fig 1.pdf

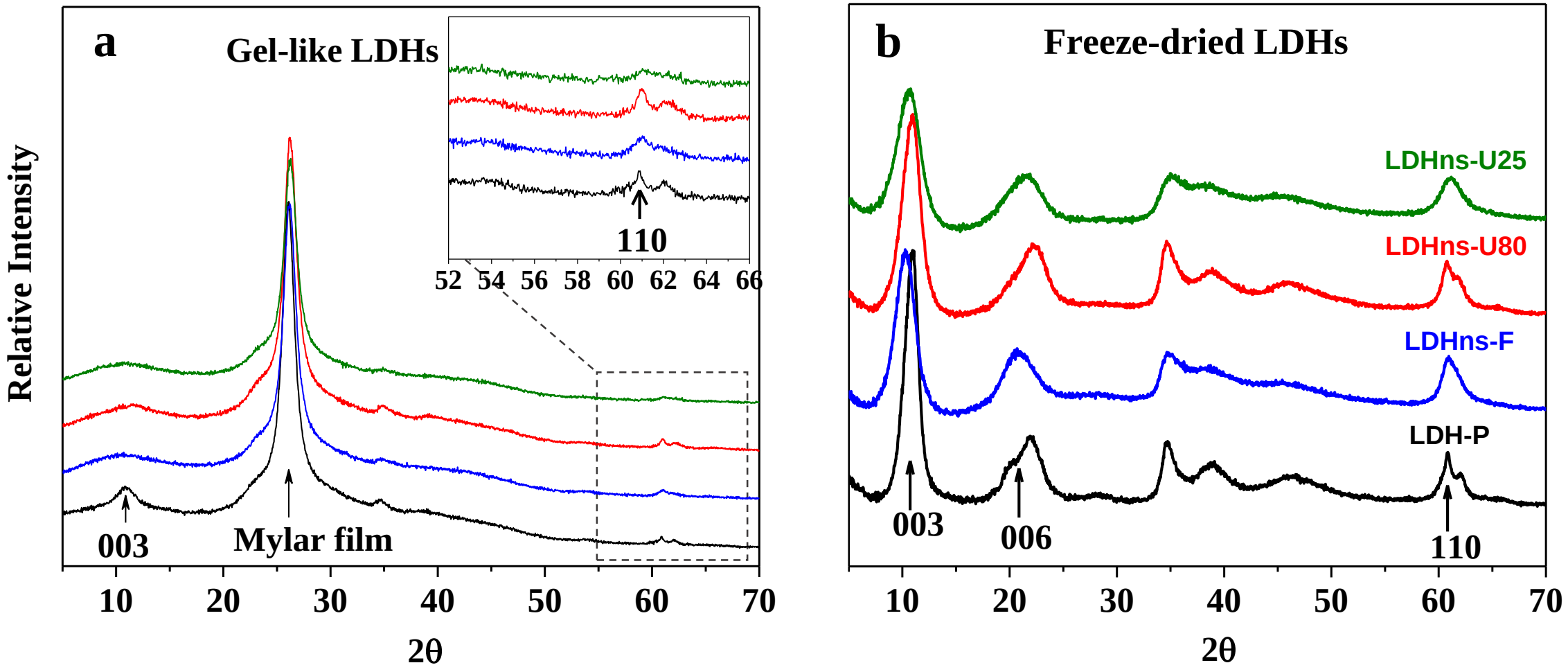

Figure
Click here to download Figure: Fig 2.pdf

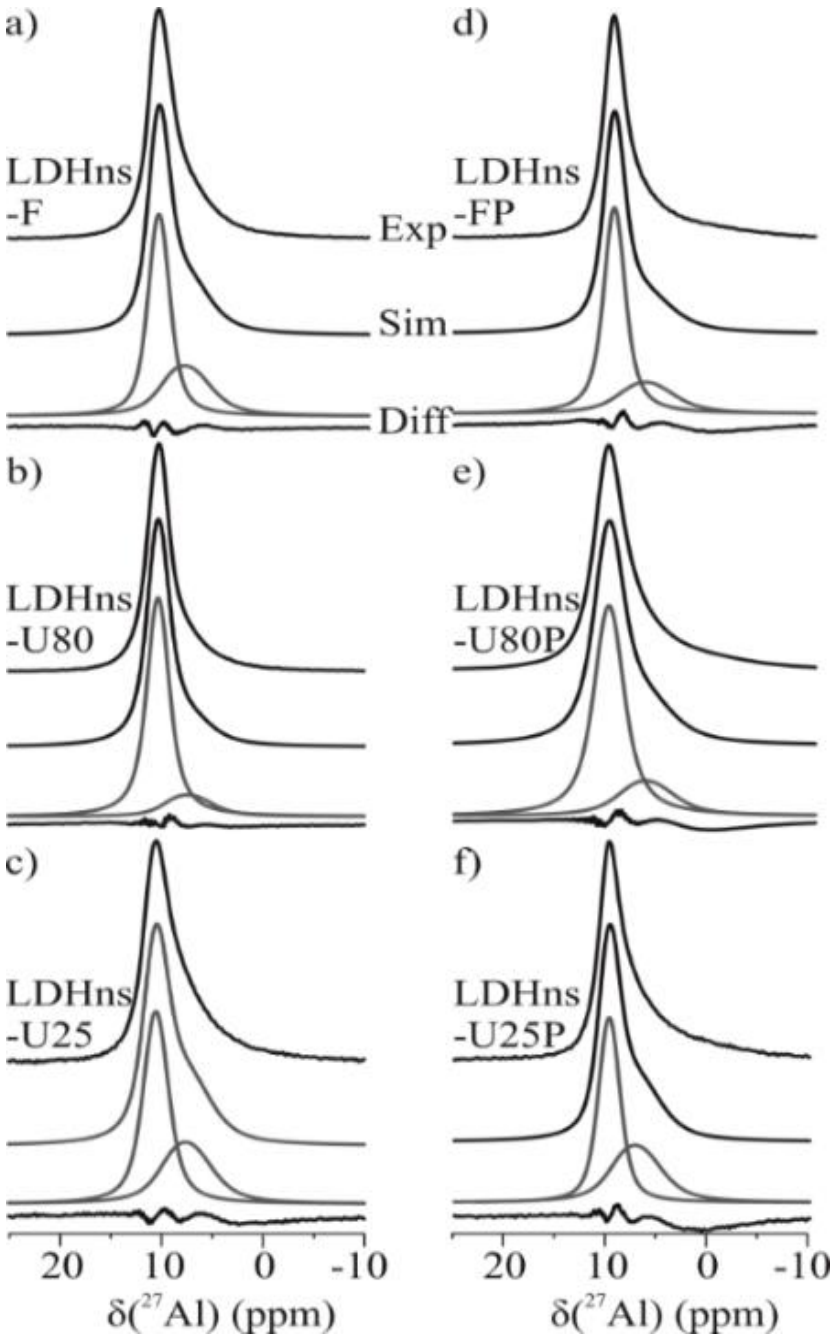

Figure
Click here to download Figure: Fig 3.pdf

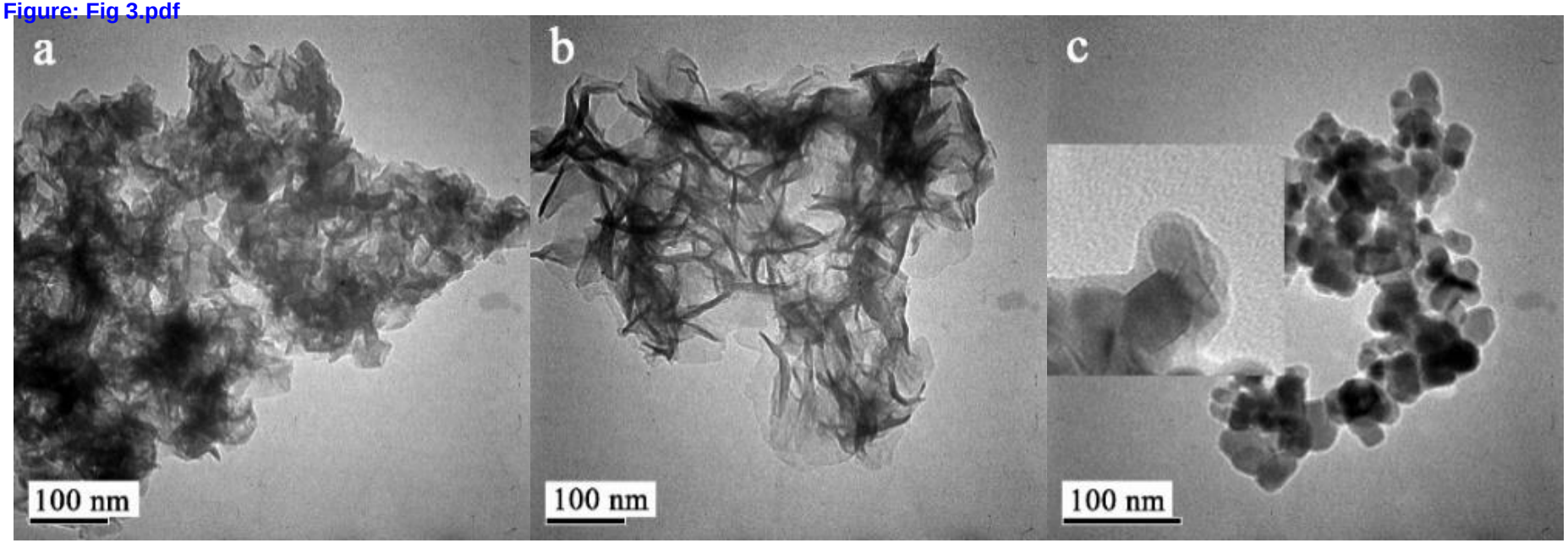

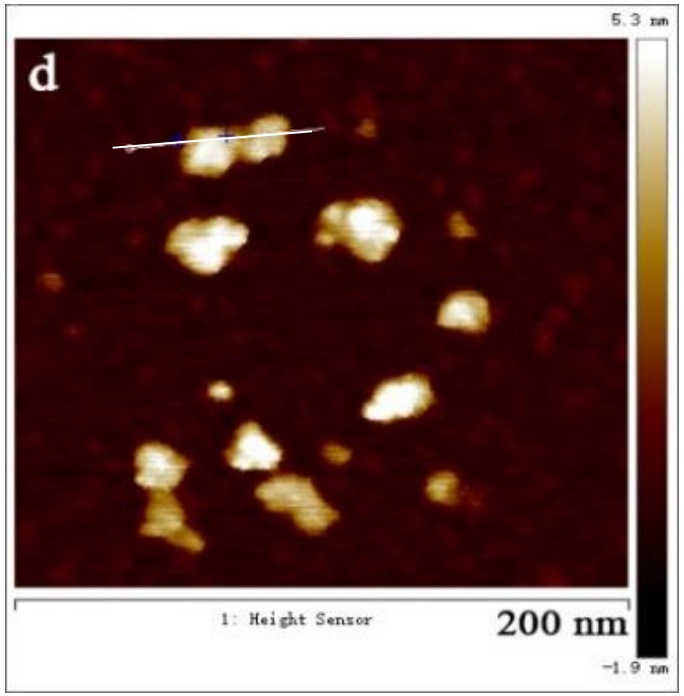

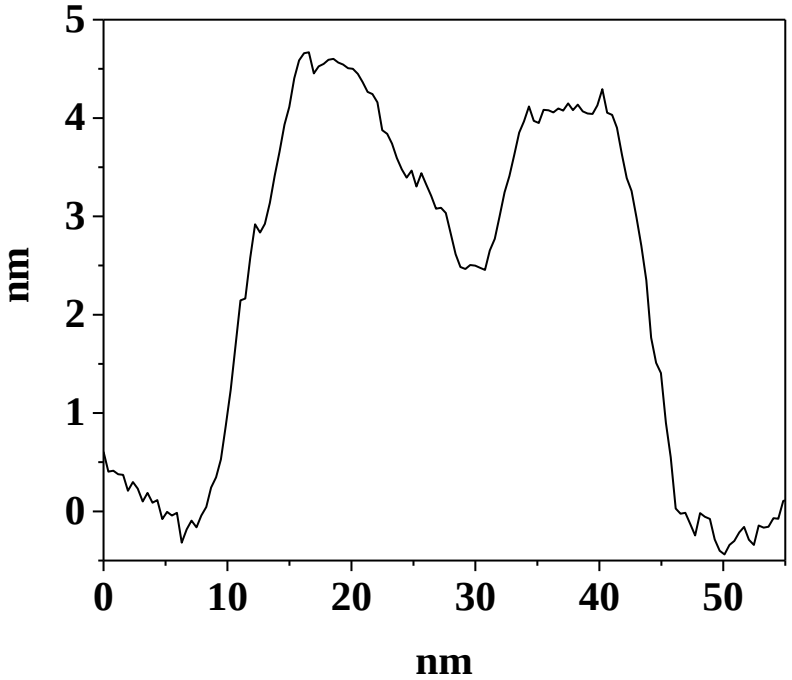

Figure
Click here to download Figure: Fig 4.pdf

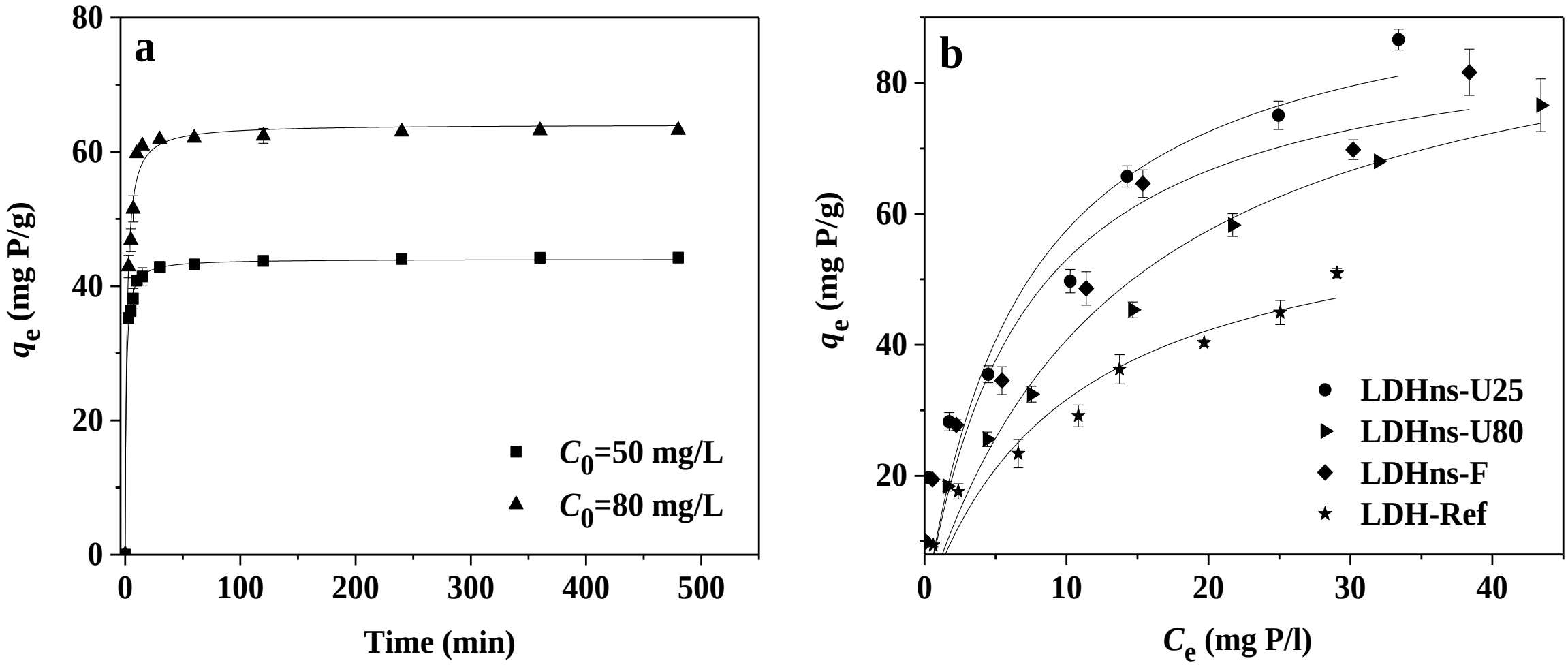

Figure
Click here to download Figure: Fig 5.pdf

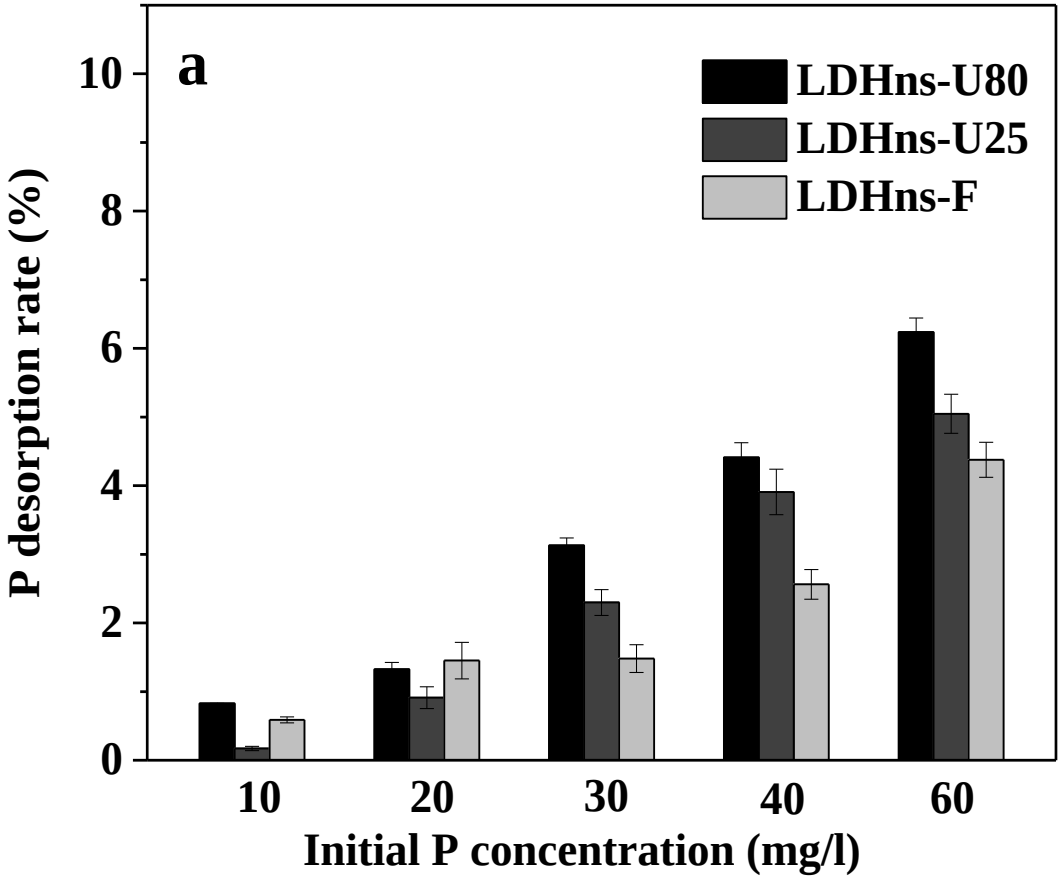

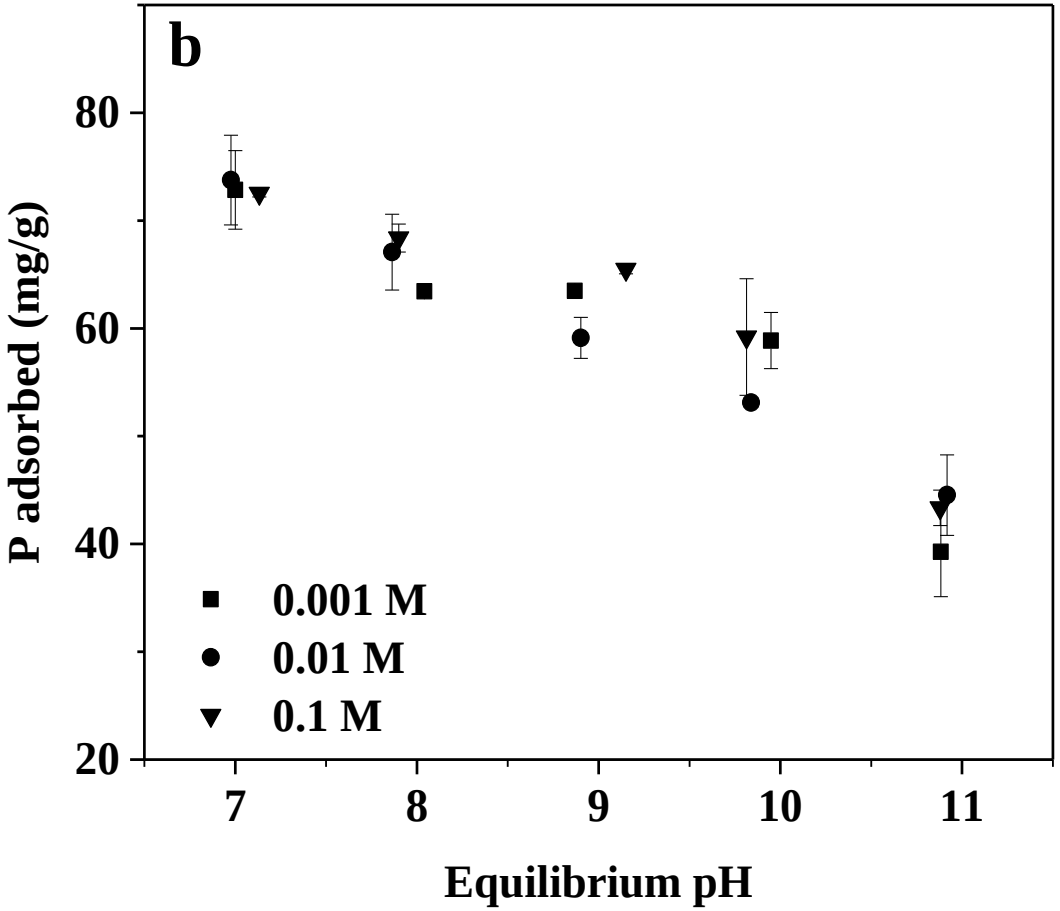

Figure
Click here to download Figure: Fig 6.pdf

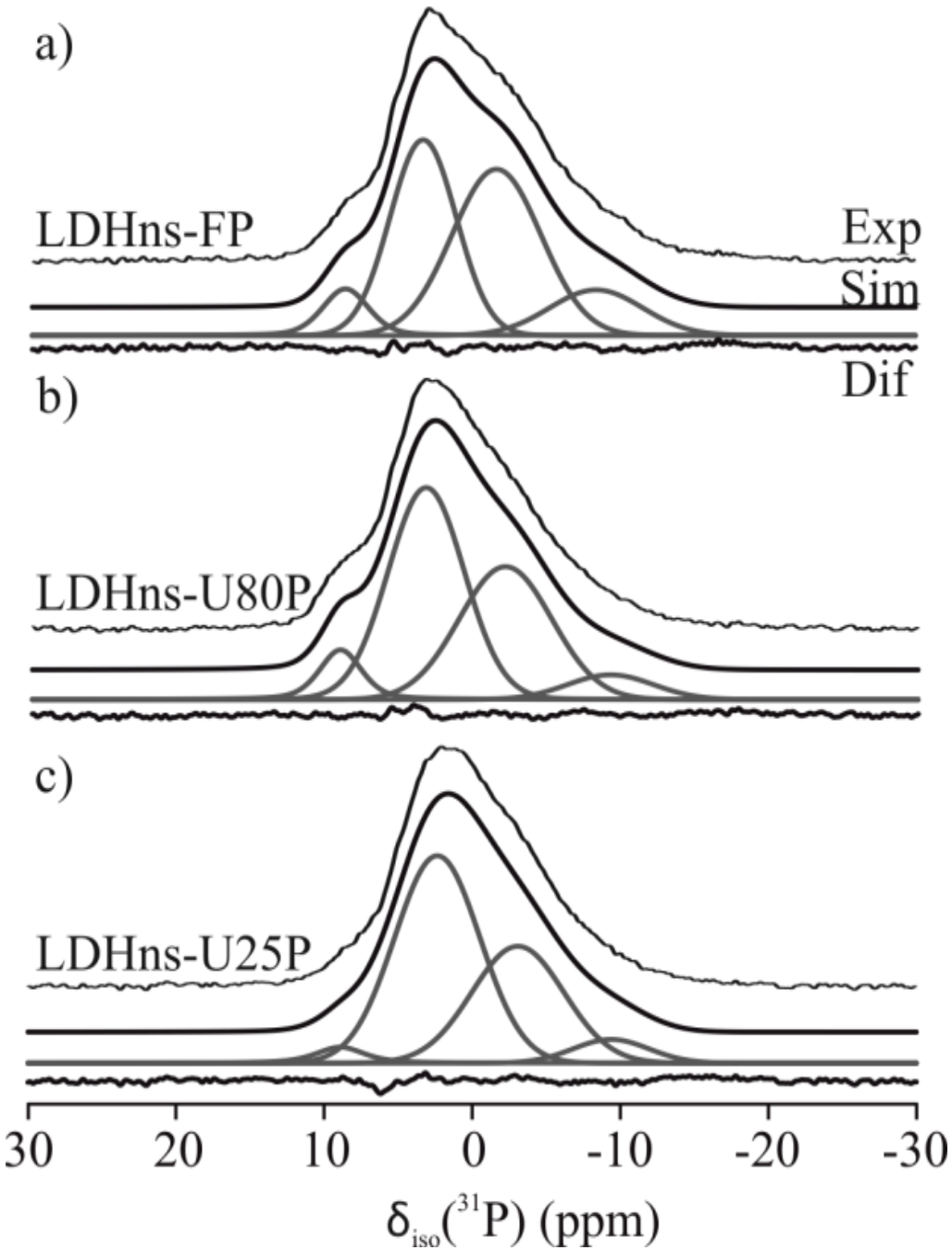

Figure
Click here to download Figure: Fig 7.pdf

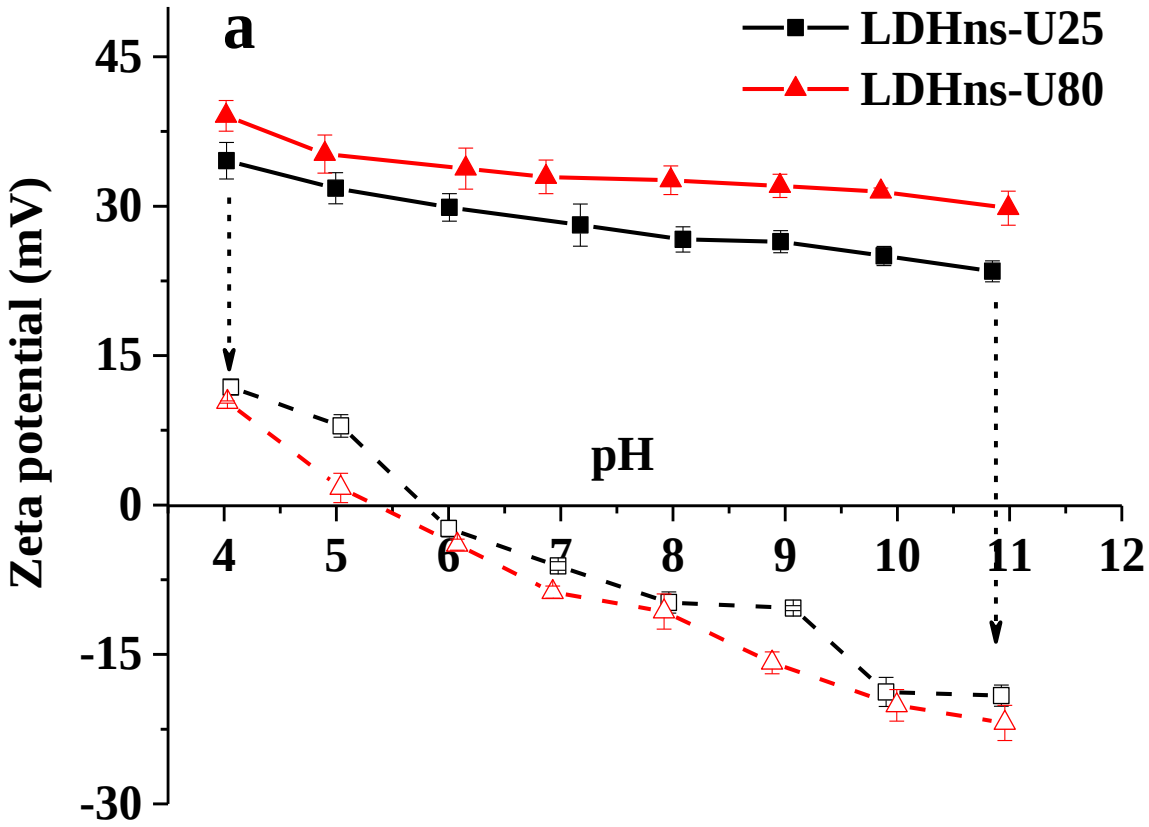

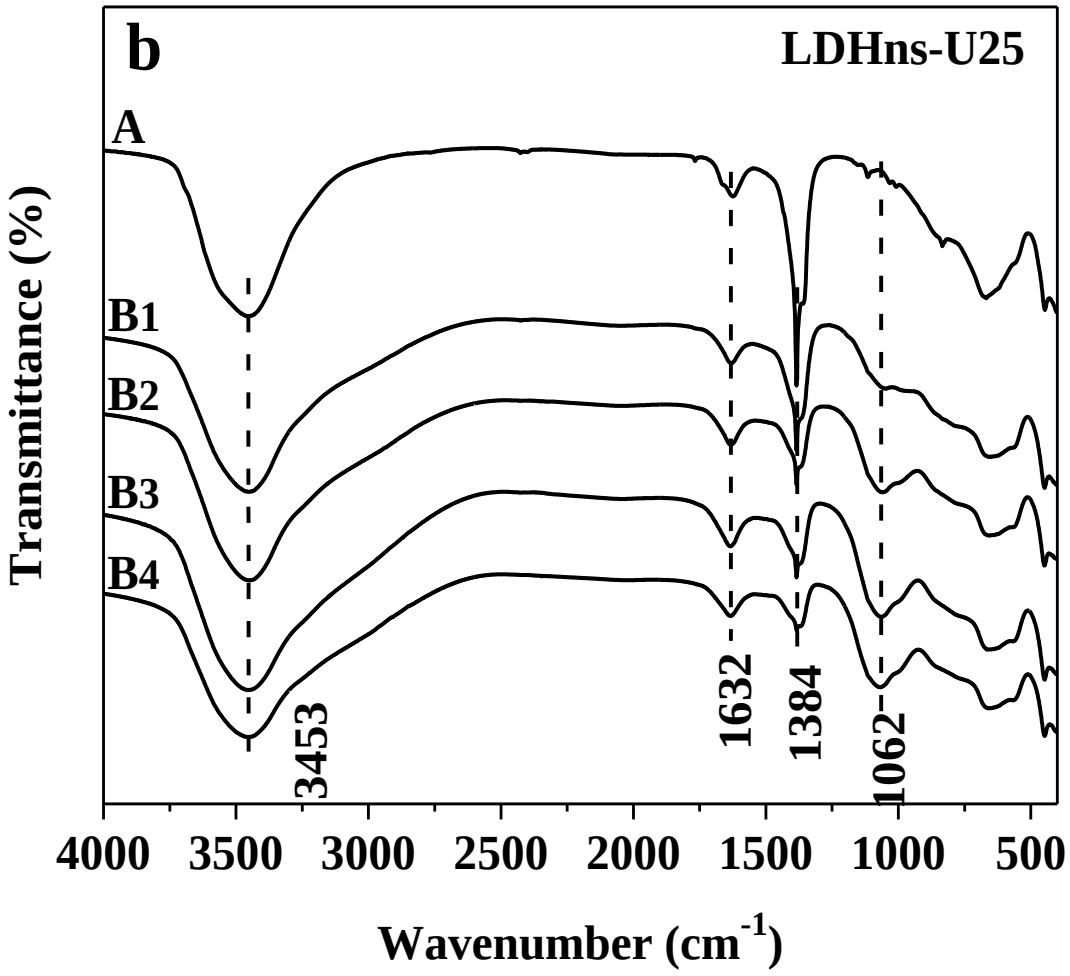

Figure
Click here to download Figure: Fig 8.pdf

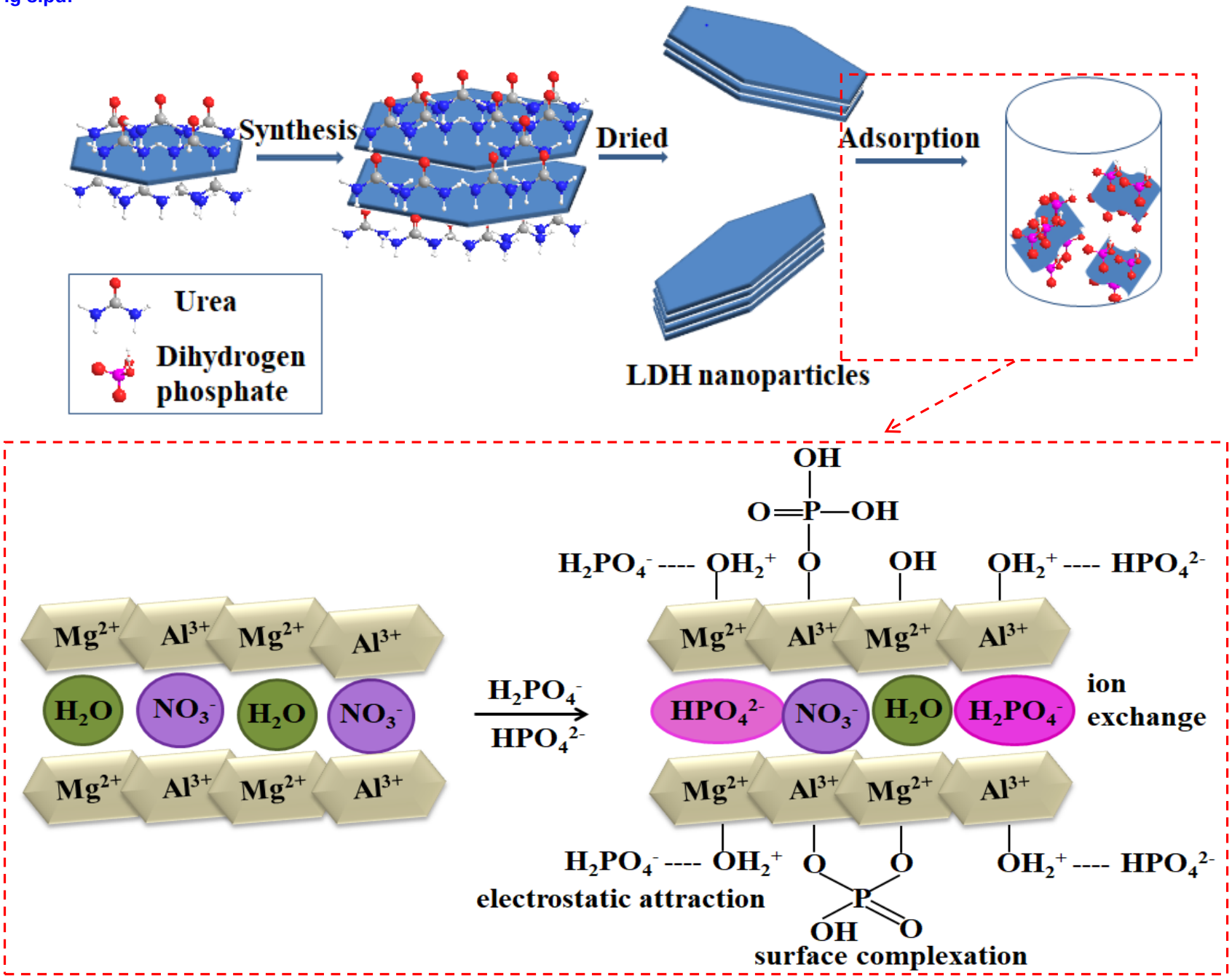

Abstract

Capture of phosphorus from runoff and wastewater is of high priority in order to reclaim phosphorus for food security and to prevent water pollution. Here we report an environmentally friendly method to synthesize ultrathin MgAl layered double hydroxide (LDH) nanoparticles for phosphorus adsorption. Fast co-precipitation of magnesium and aluminum at 25-80 °C in the presence of urea resulted in the desired LDH with variable admixtures of amorphous aluminum hydroxide (16-38%) quantified from solid state ^{27}Al MAS NMR. Freshly synthesized particles appeared as exfoliated single layers that upon drying stacked to form particles with thickness of 3 to 5 nm (four to six LDH layers) and lateral sizes of ~30 nm, as seen by XRD, SEM, TEM, and AFM. Phosphate adsorption on LDH nanoparticles synthesized at room temperature (LDHns-U25) was very fast and reaction reached equilibrium within 15 min at pH 8.5. The freeze-dried LDHns-U25 nanoparticles exhibited phosphate sorption capacity of 98±15 mg P g^{-1}, which is 55% higher than conventional LDH. Phosphate was bound to LDH electrostatically and via inner-sphere surface complexation as evidenced from a combination of ^{31}P MAS NMR spectroscopy, surface potential measurements, IR spectroscopy, and ionic strength effects on phosphate sorption. This study demonstrates that urea-facilitated synthesis of LDH nanoparticles provides fast and high capacity phosphate sorbents with potentials for phosphate recovery from waste waters.